2. Methods

2.1. Surgical preparation

Animal care was provided in strict accordance with the Guiding Principles for the Care and Use of Animals in the Field of Physiological Sciences approved by the Physiological Society of Japan. All protocols were reviewed and approved by the Animal Subject Committee at the National Cerebral and Cardiovascular Center. Male Wister Kyoto rats weighing from 310 to 460 g were anesthetized by an intraperitoneal injection of pentobarbital sodium (50 mg/kg) and ventilated mechanically via a tracheal tube with oxygen-enriched room air. The depth of anesthesia was maintained by continuous intravenous infusion of pentobarbital sodium (20–25 mg kg^{-1} h^{-1}) through a double lumen catheter inserted into the right external carotid vein. Ringer solution (6 mg kg^{-1} h^{-1}) was administered to maintain fluid balance. Arterial blood pressure (AP) was measured using a catheter inserted into the right common carotid artery. Heart rate (HR) was determined from AP using a cardiotachometer. Body temperature was maintained at approximately 38 °C using a heating pad.

2.2. MA and EA stimulations ($n=9$)

With the animal in the supine position, both hind limbs were lifted to obtain a better view of the lateral sides of the lower legs. An acupuncture needle with a diameter of 0.2 mm (CE0123, Seirin-Kasei, Japan) was inserted into a point below the knee joint just lateral to the tibia in the left or right leg. For MA stimulation, the acupuncture needle was inserted to a depth of 5–10 mm and manually twisted clockwise and counter-clockwise, and moved up and down at a frequency of 1–2 Hz for a duration of 120 s. Two to three MA trials were conducted with an intervening interval of more than 5 min within which AP and HR returned to the respective pre-stimulation values. For EA stimulation, another acupuncture needle was inserted into a point approximately 1 cm from the above-mentioned needle toward the ankle joint and used as the ground. EA was applied for 120 s using an isolator connected to an electrical stimulator (SEN 7203, Nihon Kohden, Japan). The pulse width and the stimulus current were set at 500 μs and 5 mA, respectively. The stimulation frequency was set at 10 Hz in six and at 20 Hz in three of the nine rats. The pulse duration was based on previous studies (Tjen-A-Looi et al., 2005; Yamamoto et al., 2008; Uchida et al., 2008). The amplitude and frequency were selected so that the magnitudes of reflex hemodynamic responses became comparable to those induced by MA before gadolinium administration. In each animal, two to three EA trials were conducted with an intervening interval of more than 5 min within which AP and HR returned to the respective pre-stimulation values.

Gadolinium chloride hexahydrate was dissolved in saline at a concentration of 20 mM (Nakamoto and Matsukawa, 2007). After performing MA and EA under control conditions, we administered the gadolinium solution intravenously (2 ml/kg). After 10 min, we repeated MA and EA. The acupuncture needle positions were kept unchanged between MA and EA trials as well as before and after the gadolinium administration.

In a supplemental protocol ($n=7$ additional rats), to examine the possibility that simple insertion of needles caused significant hemodynamic influences, an acupuncture needle (CE0123, Seirin-Kasei, Japan) was only inserted into a point below the knee joint just lateral to the tibia in the left or right leg and placed for a duration of 120 s. Needle was inserted to a depth of 5–10 mm.

2.3. Aortic depressor nerve stimulation ($n=6$)

Using a pair of platinum electrodes, we identified the aortic depressor nerve (ADN) running along the common carotid artery, based on the AP pulse-synchronous nerve activity monitored through a loud speaker. After a depressor response to brief electrical stimulation of the nerve was confirmed, the electrodes and the nerve were fixed and insulated by silicone glue (Kwik-Sil, World Precision Instruments, FL, USA). The nerve fibers caudal to the electrodes were then crushed by a tight ligature so that only the afferent fibers directed to the central nervous system were stimulated. In four of the six rats, the right ADN was stimulated. In the remaining two rats, the left ADN was stimulated because of failure to stimulate the right ADN properly. The ADN was stimulated for 120 s at a frequency of 50 Hz (pulse width: 2 ms, voltage: 2 V). ADN stimulation was repeated with an interval of 5 min until the AP and HR responses appeared to be reproducible under control conditions. We then administered the gadolinium solution intravenously (20 mM, 2 ml/kg). After 10 min, we repeated the ADN stimulation.

2.4. Data analysis

Data were digitized using a 16-bit analog-to-digital converter (Contec, Japan) and stored at 200 Hz on a laboratory computer system. First, AP and HR data were averaged every 10 s. Averaged time courses of AP and HR responses were then obtained from two to three trials of MA, EA or ADN stimulation in each animal. Next, the effects of MA, EA or ADN were examined using repeated-measures one-way analysis of variance (ANOVA) followed by Dunnett's test (Glantz, 2002). The baseline data point immediately before stimulation was treated as a single control point for the Dunnett's test. Finally, the maximum effect of MA, EA or ADN stimulation was quantified by the differences between the minimum and baseline values for AP and HR (ΔAP and ΔHR). The effects of gadolinium on ΔAP and ΔHR were examined by a paired-t test (Glantz, 2002). The differences were considered significant at $P<0.05$. Data are presented in mean ± SE values.

3. Results

Fig. 1 depicts the averaged time courses of AP and HR responses to MA ($n=9$ rats). MA gradually decreased AP and HR under control conditions. The minimum AP and HR were reached near the end of the MA stimulation period. After the cessation of MA, AP and HR gradually returned toward the respective baseline values. Intravenous gadolinium administration significantly decreased baseline AP from 138 ± 5 to 120 ± 5 mm Hg ($P<0.01$) but had no significant effect on baseline HR (379 ± 10 vs. 383 ± 7 bpm). Following gadolinium administration, although MA also decreased AP and HR significantly, ΔAP tended to be attenuated (−30 ± 5 vs. −18 ± 4 mm Hg; 68 ± 16% of the pre-gadolinium; $P=0.06$) and ΔHR was significantly attenuated (−22 ± 5 vs. −10 ± 3 bpm; 57 ± 23% of the pre-gadolinium; $P<0.05$) compared to control conditions.

Fig. 2 depicts the averaged time courses of AP and HR responses to EA ($n=9$ rats). Under control conditions, EA decreased AP and HR. Both responses reached almost a steady state at approximately 1 min of EA stimulation. AP and HR remained decreased during the rest of the EA stimulation period, and gradually returned toward the respective baseline values after the cessation of EA. Intravenous gadolinium administration significantly decreased baseline AP from 140 ± 5 to 123 ± 7 mm Hg ($P<0.01$) but did not affect baseline HR (385 ± 9 vs. 384 ± 7 bpm). Following gadolinium administration, although EA significantly decreased AP, the decrease in HR was only significant at 55 s of EA stimulation. ΔAP (−32 ± 6 vs. −15 ± 5 mm Hg; 38 ± 11% of the pre-gadolinium; $P<0.01$) and ΔHR (−22 ± 5 vs. −9 ± 4 bpm; 37 ± 14% of the pre-gadolinium; $P<0.01$) were attenuated significantly compared to control conditions.

In the supplemental protocol ($n=7$ rats), the insertion of an acupuncture needle alone did not significantly change AP (138 ± 9 vs. 138 ± 9 mm Hg) or HR (399 ± 20 vs. 400 ± 20 bpm).

Fig. 3 shows the averaged time courses of AP and HR responses to ADN stimulation ($n=6$ rats). ADN stimulation decreased AP and HR under control conditions. The minimum AP and HR were reached at 15 s of ADN stimulation. Both parameters remained decreased during the rest of the ADN stimulation period, and returned toward the respective

Please cite this article as: Yamamoto, H., et al., Involvement of the mechanoreceptors in the sensory mechanisms of manual and electrical acupuncture, Auton. Neurosci. (2010), doi:10.1016/j.autneu.2010.11.004

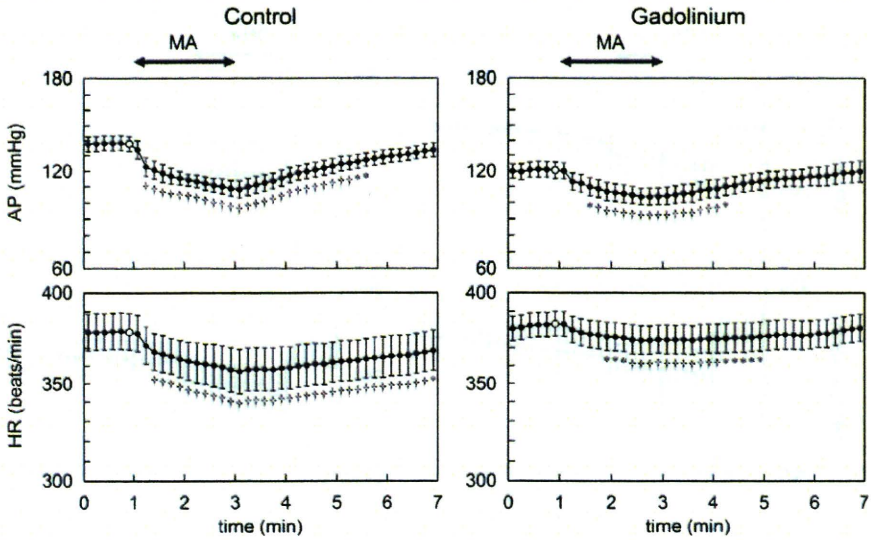

Fig. 1. Time courses of arterial pressure (AP) and heart rate (HR) responses induced by manual acupuncture (MA) averaged from 9 rats. MA gradually decreased AP and HR under control conditions (left) and after gadolinium administration (right). Gadolinium treatment tended to attenuate the AP response and significantly attenuated the HR response induced by MA, compared to control conditions. Data are mean ± SE values. $^{*}P<0.05$ and $^{\dagger}P<0.01$ versus the control data point (open circle) immediately before the application of MA.

baseline values after the cessation of ADN stimulation. AP and HR appeared to recover more rapidly compared to those observed after MA and EA. Intravenous gadolinium administration significantly decreased baseline AP from 126 ± 4 to 118 ± 2 mm Hg ($P<0.01$) but had no significant effect on baseline HR (373 ± 13 vs. 369 ± 11 bpm). Following gadolinium administration, ADN stimulation significantly decreased AP and HR. Neither ΔAP (−43 ± 7 vs. −49 ± 3 mm Hg) nor ΔHR (−27 ± 8 vs. −34 ± 5 bpm) was attenuated compared to control conditions.

4. Discussion

We have shown that ion channels blocked by gadolinium are implicated in the hypotensive and bradycardic effects of acupuncture at the hind limb in rats, irrespective of technique.

4.1. Effects of gadolinium on AP and HR responses to MA and EA

Insertion of acupuncture needle alone did not change AP and HR significantly, indicating that continuous stimulation either by MA or EA was necessary to induce sustained AP and HR responses. Mechanoreceptors are thought to play an important role in the sensory mechanism of MA. Because gadolinium blocks mechanosensitive ion channels in sensory neurons (Cho et al., 2002), we hypothesized that intravenous administration of gadolinium would attenuate the AP and HR responses to MA. As expected, ΔAP tended to be attenuated after gadolinium administration (Fig. 1, top). However, since gadolinium also decreased baseline AP, it is uncertain whether the attenuation of ΔAP was mainly attributable to the inhibition of reflex response to MA or to the decreased baseline AP. On the other hand, gadolinium did not significantly affect baseline HR and

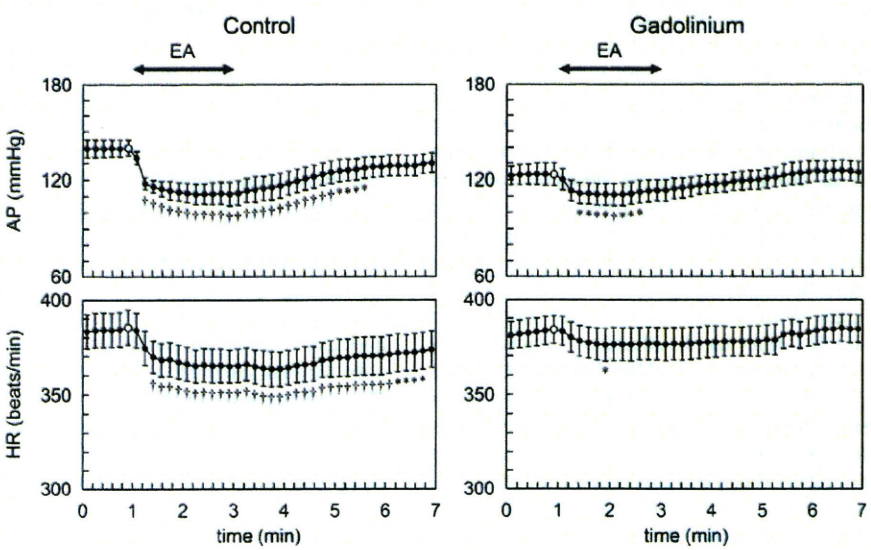

Fig. 2. Time courses of AP and HR responses induced by electroacupuncture (EA) averaged from 9 rats. EA gradually decreased AP and HR under control conditions (left) and after gadolinium administration (right). Gadolinium significantly attenuated both AP and HR responses induced by EA, compared to control conditions. Data are mean ± SE values. $^{*}P<0.05$ and $^{\dagger}P<0.01$ versus the control data point (open circle) immediately before the application of EA.

Please cite this article as: Yamamoto, H., et al., Involvement of the mechanoreceptors in the sensory mechanisms of manual and electrical acupuncture, Auton. Neurosci. (2010), doi:10.1016/j.autneu.2010.11.004

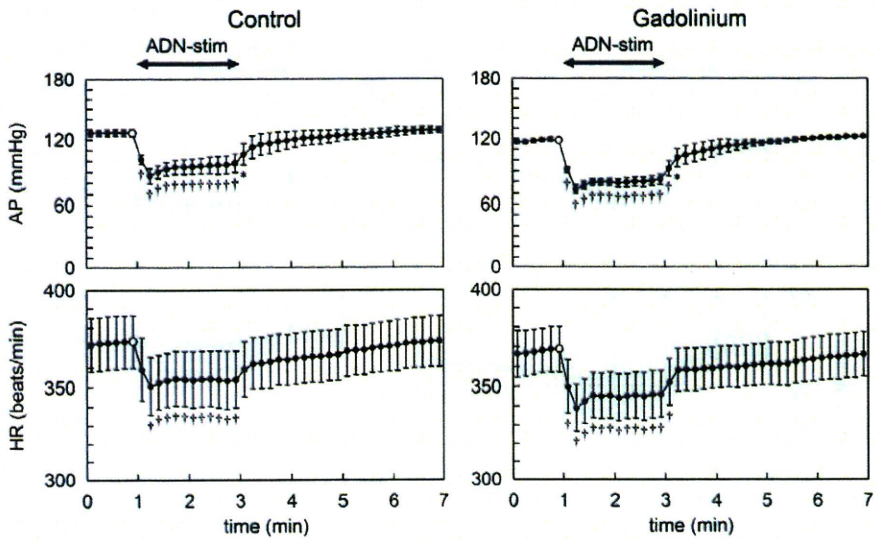

Fig. 3. Time courses of AP and HR responses induced by electrical stimulation of the aortic depressor nerve (ADN-stim) averaged from 6 rats. ADN-stim decreased AP and HR under control conditions (left) and after gadolinium administration (right). Gadolinium did not attenuate the AP and HR responses induced by ADN-stim, compared to control conditions. Data are mean ± SE values. $^{*}P<0.05$ and $^{\dagger}P<0.01$ versus the control data point (open circle) immediately before the application of ADN-stim.

significantly attenuated ΔHR induced by MA (Fig. 1, bottom). Judging from the HR response, it is conceivable that gadolinium inhibits the reflex hemodynamic responses to MA.

We assumed that direct depolarization of sensory axons and nerve terminals adjacent to the needle could be the major sensory mechanism of EA. In fact, direct electrical stimulation of muscle afferent fibers evokes a variety of cardiovascular responses similar to those induced by EA (Sato et al., 1981). If direct depolarization is the major sensory mechanism for EA, inhibition of mechanoreceptors would have no significant effect on EA, because the results of the ADN stimulation protocol indicates that the axonal conduction would not be blocked even after gadolinium administration once the afferent nerve is discharged (Fig. 3). Contrary to this assumption, gadolinium significantly attenuated ΔAP and ΔHR induced by EA (Fig. 2), suggesting that the mechanoreceptors play an important role in the sensory mechanism of EA, as in the case of MA. EA probably causes electrical twitching of surrounding tissues and exerts MA-like stimulation through the mechanoreceptors.

Despite the significant contribution of mechanoreceptors to the sensory mechanisms of both MA and EA, the fact that the hemodynamic responses to MA and EA were not entirely abrogated after gadolinium administration indicates the presence of sensory mechanisms other than the mechanosensitive ion channels. Not all capsaicin-sensitive neurons are mechanosensitive, and gadolinium has no effect on capsaicin-induced calcium transient in sensory neurons (Gschossmann et al., 2000). Depletion of group IV fibers by neonatal capsaicin treatment reduces the influence of EA on the pressor responses to mechanical stimulation of visceral organs (Tjen-A-Looi et al., 2005), suggesting an importance of capsaicin-sensitive neurons in the mechanisms of acupuncture. Nociceptive neurons are therefore a likely candidate for the residual sensory mechanism after gadolinium administration. The group IV C-fiber tactile afferents is known to be widely distributed in the skin of mammals (Wessberg et al., 2003). These fibers could be regarded as a cutaneous intrinsic visceral afferent nervous system (Silberstein, 2009). In addition, the present results do not rule out the possibility that direct depolarization of sensory axons or nerve terminals occurs during EA. Albeit this assumption, EA seemed to have received even greater influence from gadolinium than MA (Figs. 1 and 2). Because MA with needle movements can cause greater deformations in the adjacent extracellular milieu compared to EA, MA may have induced signal transductions other than mechanosensitive ion channels, such as integrin-linked signal transduction pathways (Aplin et al., 1998), resulting in the greater residual hemodynamic responses after gadolinium administration. Further studies are required in the future to solve this question.

4.2. Effects of gadolinium on the AP and HR responses to ADN stimulation

Gadolinium decreased baseline AP, suggesting actions other than the inhibition of mechanosensitive ion channels. For instance, gadolinium has been shown to block voltage-gated calcium, sodium and potassium channels (Adding et al., 2001). To exclude the possibility that gadolinium attenuates the reflex hemodynamic responses to MA and EA via nonspecific mechanisms such as the inhibition of central autonomic neurotransmission, we performed the ADN stimulation experiment. Gadolinium did not attenuate ΔAP and ΔHR induced by ADN stimulation (Fig. 3). It is unlikely, therefore, that gadolinium inhibits the central autonomic neurotransmission from afferent to efferent nerve activities or significantly blunted the AP and HR responses to changes in autonomic nerve activities.

4.3. Implication of MA and EA

Although the present results indicate that MA and EA may share a common sensory mechanism, EA may be more flexible than MA in terms of its application for biomedical engineering because the effects of EA can be controlled quantitatively by adjusting the stimulation current and stimulation frequency. As an example, a previous study from our laboratories has demonstrated that servo-controlled hind limb electrical stimulation can reduce AP at a prescribed target level in anesthetized cats (Kawada et al., 2009). EA can be applied continuously using a stimulating device without the attendance of an acupuncturist once the needle is properly positioned. Continuous electrical stimulation of auricular acupuncture points for 48 h/week has been shown to be more effective than auricular acupuncture without electrical stimulation for the treatment of chronic cervical pain in an outpatient population (Sator-Katzenschlager et al., 2003). Although further studies are required, EA delivered via a dedicated stimulating device may be an additional modality to the treatment of cardiovascular diseases.

4.4. Limitations

First, the present study was conducted under pentobarbital anesthesia. Because anesthesia affects the autonomic tone, AP and HR

Please cite this article as: Yamamoto, H., et al., Involvement of the mechanoreceptors in the sensory mechanisms of manual and electrical acupuncture, Auton. Neurosci. (2010), doi:10.1016/j.autneu.2010.11.004

responses may differ when different anesthetics are used or when the animals are in a conscious state. However, as we compared the effects of gadolinium on the reflex responses to MA and EA under the same anesthetic conditions, the interpretation of the sensory mechanisms for MA and EA should be valid. Second, we performed EA at frequencies of 10 or 20 Hz in order to obtain AP and HR responses comparable to those observed during MA under control conditions. Because the effects of EA may differ depending on the magnitude of stimulation including pulse duration, current and frequency (Uchida et al., 2008; Kawada et al., 2009), further studies are needed to examine whether the effects of gadolinium on EA-induced hemodynamic responses vary depending on the stimulation intensities.

4.5. Conclusion

Intravenous administration of gadolinium attenuated the AP and HR responses to both MA and EA, suggesting that the mechanosensitive ion channels are involved in the sensory mechanisms of both MA and EA. EA may cause electrical twitching of surrounding tissues and induce MA-like stimulation through mechanoreceptors.

Acknowledgments

This study was supported by Health and Labour Sciences Research Grants (H19-nano-Ippan-009, H20-katsudo-Shitei-007, and H21-nano-Ippan-005) from the Ministry of Health, Labour and Welfare of Japan; by a Grant-in-Aid for Scientific Research (No. 20390462) from the Ministry of Education, Culture, Sports, Science and Technology of Japan; and by the Industrial Technology Research Grant Program from the New Energy and Industrial Technology Development Organization (NEDO) of Japan.

Appendix A

In an attempt to demonstrate that gadolinium does not significantly affect the hemodynamic responses to direct nerve stimulation related to acupuncture at the hind limb, we performed an additional protocol of tibial nerve stimulation in 5 anesthetized rats. The right tibial nerve was exposed and placed on a pair of platinum electrodes, and was stimulated for 120 s (500 μs, 10 Hz, 2 or 5 mA). ΔAP was -10.5 ± 3.5 mm Hg under baseline conditions, which was attenuated to -8.2 ± 4.4 mm Hg after gadolinium administration ($74 \pm 15\%$ of the pre-gadolinium, $P < 0.01$). Although the relative reduction seemed smaller than that observed in EA ($38 \pm 11\%$ of the pre-gadolinium, see main text), because the reduction of ΔAP could be partly attributable to the decreased baseline AP after gadolinium administration, we could not judge whether gadolinium had truly inhibited the hypotensive effect of tibial nerve stimulation. Unfortunately, the tibial nerve stimulation did not change HR significantly in our experimental conditions ($\Delta HR = -1.1 \pm 4.4$ bpm before gadolinium vs. $\Delta HR = -1.4 \pm 4.1$ bpm after gadolinium), as opposed to a previous study (Uchida et al., 2008). As a result, we could not judge the effect of gadolinium based on HR either. We think the ADN stimulation protocol in the main text would be a second best surrogate to indicate the inability of gadolinium to block hemodynamic responses induced by direct activation of the afferent nerve.

References

Adding, L.C., Bannenberg, G.L., Gustafsson, L.E., 2001. Basic experimental studies and clinical aspects of gadolinium salts and chelates. Cardiovasc. Drug Rev. 19, 41–56.
Aplin, A.E., Howe, A., Alahari, S.K., Juliano, R.L., 1998. Signal transduction and signal modulation by cell adhesion receptors: the role of integrins, cadherins, immunoglobulin-cell adhesion molecules, and selectins. Pharmacol. Rev. 50 (2), 197–263.
Burnstock, G., 2009. Acupuncture: a novel hypothesis for the involvement of purinergic signalling. Med. Hypotheses 73, 470–472.
Cho, H., Shin, J., Shin, C.Y., Lee, S., Oh, U., 2002. Mechanosensitive ion channels in cultured sensory neurons of neonatal rats. J. Neurosci. 22 (4), 1238–1247.
Glantz, S.A., 2002. Primer of Biostatistics, 5th ed. McGraw-Hill, New York.
Gschossmann, J.M., Chaban, V.V., McRoberts, J.A., Raybould, H.E., Young, S.H., Ennes, H.S., Lembo, T., Mayer, E.A., 2000. Mechanical action of dorsal root ganglion cells in vitro: comparison with capsaicin and modulation by kappa-opioids. Brain Res. 856 (1–2), 101–110.
Kawada, T., Shimizu, S., Yamamoto, T., Shishido, T., Kamiya, A., Miyamoto, T., Sunagawa, K., Sugimachi, M., 2009. Servo-controlled hind-limb electrical stimulation for short-term arterial pressure control. Circ. J. 73 (5), 851–859.
Kimura, A., Sato, A., 1997. Somatic regulation of autonomic functions in anesthetized animals—neural mechanisms of physical therapy including acupuncture. Jpn J. Vet. Res. 45 (3), 137–145.
Langevin, H.M., Churchill, D.L., Cipolla, M.J., 2001. Mechanical signaling through connective tissue: a mechanism for the therapeutic effect of acupuncture. FASEB J. 15, 2275–2285.
Lin, M.C., Nahin, R., Gershwin, M.E., Longhurst, J.C., Wu, K.K., 2001. State of complementary and alternative medicine in cardiovascular, lung, and blood research: executive summary of a workshop. Circulation 103 (16), 2038–2041.
Nakamoto, T., Matsukawa, K., 2007. Muscle mechanosensitive receptors close to the myotendinous junction of the Achilles tendon elicit a pressor reflex. J. Appl. Physiol. 102, 2112–2120.
Napadow, V., Makris, N., Liu, J., Kettner, N.W., Kenneth, K.K., Hui, K.K.S., 2005. Effects of electroacupuncture versus manual acupuncture on the human brain as measured by fMRI. Hum. Brain Mapp. 24, 193–205.
Sato, A., Sato, Y., Schmidt, R.F., 1981. Heart rate changes reflecting modifications of efferent cardiac sympathetic outflow by cutaneous and muscle afferent volleys. J. Auton. Nerv. Syst. 4 (3), 231–247.
Sato, A., Sato, Y., Suzuki, A., Uchida, S., 1994. Reflex modulation of gastric and vesical function by acupuncture-like stimulation in anesthetized rats. Biomed. Res. 15, 59–65.
Sato, A., Sato, Y., Uchida, S., 2002. Reflex modulation of visceral functions by acupuncture-like stimulation in anesthetized rats. Int. Congr. Ser. 1238, 111–123.
Sator-Katzenschlager, S.M., Szeles, J.C., Scharbert, G., Michalek-Sauberer, A., Kober, A., Heinze, G., Kozek-Langenecker, S.A., 2003. Electrical stimulation of auricular acupuncture points is more effective than conventional manual auricular acupuncture in chronic cervical pain: a pilot study. Anesth. Analg. 97, 1469–1473.
Silberstein, M., 2009. The cutaneous intrinsic visceral afferent nervous system: a new model for acupuncture analgesia. J. Theor. Biol. 261, 637–642.
Tjen-A-Looi, S.C., Fu, L.-W., Zhou, W., Syuu, Z., Longhurst, J.C., 2005. Role of unmyelinated fibers in electroacupuncture cardiovascular responses. Auton. Neurosci. 118, 43–50.
Uchida, S., Shimura, M., Ohsawa, H., Suzuki, A., 2007. Neural mechanism of bradycardic responses elicited by acupuncture-like stimulation to a hind limb in anesthetized rats. J. Physiol. Sci. 57 (6), 377–382.
Uchida, S., Kagitani, F., Hotta, H., 2008. Mechanism of the reflex inhibition of heart rate elicited by acupuncture-like stimulation in anesthetized rats. Auton. Neurosci. 143, 12–19.
Wessberg, J., Olausson, H., Fernstrom, W.F., Vallbo, B.A., 2003. Receptive field properties of unmyelinated tactile afferents in the human skin. J. Neurophysiol. 89, 1567–1575.
Yamamoto, H., Kawada, T., Kamiya, A., Kita, T., Sugimachi, M., 2008. Electroacupuncture changes the relationship between cardiac and renal sympathetic nerve activities in anesthetized cats. Auton. Neurosci. 144 (1–2), 43–49.

Please cite this article as: Yamamoto, H., et al., Involvement of the mechanoreceptors in the sensory mechanisms of manual and electrical acupuncture, Auton. Neurosci. (2010), doi:10.1016/j.autneu.2010.11.004

32nd Annual International Conference of the IEEE EMBS
Buenos Aires, Argentina, August 31 - September 4, 2010

Development of artificial bionic baroreflex system

Kenji Sunagawa, *Senior Member, IEEE* and Masaru Sugimachi, *Member, IEEE*

***Abstract*—The baroreflex system is the fastest mechanism in the body to regulate arterial pressure. Because the neural system (i.e., autonomic nervous system) mediates the baroreflex and the system operates under the closed-loop condition, the quantitative dynamic characteristics of the baroreflex system remained unknown until recently despite the fact that a countless number of observational and qualitative studies had been conducted. In order to develop the artificial baroreflex system, i.e., the bionic baroreflex system, we first anatomically isolated the carotid sinuses to open the baroreflex loop and identified the open-loop transfer function of the baroreflex system using white noise pressure perturbations. We found that the baroreflex system is basically a lowpass filter and remarkably linear. As an actuator to implement the bionic baroreflex system, we then stimulated the sympathetic efferent nerves at various parts of the baroreflex loop and identified the transfer functions from the stimulation sites to systemic arterial pressure. We found that the actuator responses can be described remarkably well with linear transfer functions. Since transfer functions of the native baroreflex and of the actuator were identified, the controller that is required to reproduce the native baroreflex transfer function can be easily derived from those transfer functions. To examine the performance of bionic baroreflex system, we implemented it animal models of baroreflex failure. The bionic baroreflex system restored normal arterial pressure regulation against orthostatic stresses that is indistinguishable from the native baroreflex system.**

I. Introduction

Baroreflex is known to be the fastest mechanism in the body to stabilize arterial pressure. The reflex makes use of negative feedback mechanism. The baroreceptors sitting in the arterial wall sense arterial pressure and send the pressure signal to the brainstem through the afferent nerve fibers. The brainstem receives the pressure signal and judges the level of arterial pressure. If the level is low, the brainstem activates the sympathetic system innervating the heart and vascular system to increase arterial pressure. If the level of arterial pressure is high, the brainstem withdraws the sympathetic activation.

The baroreflex system is critically important in animal, particularly in human. This is because, unlike animals with four legs, the position dependent gravitational effect on circulation is most prominent in human. It is well known that once we lose the normal function of baroreflex, we no longer keep sitting and/or standing positions because of position induced profound hypotension and hypoperfusion of the brain. Baroreflex failure destroys normal life and is a devastating pathological state in human. However, since the baroreflex failure is a disease of the neural system, no effective treatment has ever developed to save those patients.

Baroreflex failure could happen under various conditions. In some patients, they lost baroreflex function because they have problems in the baroreceptors, the brainstem and/or the spinal cord. In those patients, if we can develop a mechanism to activate their sympathetic efferent system in response to changes in arterial pressure just like the native brainstem does, in theory, normal baroreflex function can be restored.

The purpose of this investigation is to develop an artificial baroreflex system, so called the bionic baroreflex system, to restore normal baroreflex function to overcome such a serious pathological condition.

II. Bionic Baroreflex System

Shown in Fig. 1 are how we identify the transfer function of the controller of bionic baroreflex system. First we identify the transfer function of the baroreflex open loop (H_{NATIVE}) from baroreceptor pressure to arterial pressure responses. We then electrically stimulate a particular site in the baroreflex loop and identify the transfer function of the actuator from the stimulation to arterial pressure responses ($H_{STM-AOP}$). Since the controller will be in series with the actuator, the transfer function of bionic baroreflex system becomes identical to the native baroreflex system when the transfer function of controller (H_{BIONIC}) satisfies the following equation:

$$H_{NATIVE} = H_{BIONIC} \times H_{STM-AOP}$$

In theory both H_{NATIVE} and $H_{STM-AOP}$ can be experimentally determined. Therefore, H_{BIONIC} can be determined. However whether such a simple approach works or not highly depends on the simplicity of the native baroreflex system including the system linearity. We therefore examined the dynamic characteristics of baroreflex system.

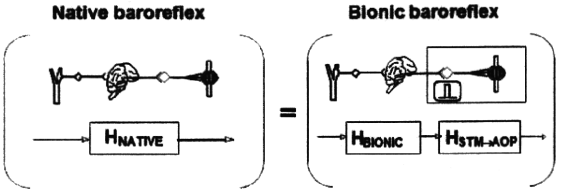

Fig. 1 Native vs. Bionic baroreflex

We vascularily isolated the baroreceptors (carotid sinuses) in rats (n=10) to open the baroreflex feedback loop and connected the carotid sinuses to a servo-controlled piston pump. This preparation allowed us to manipulate the carotid sinus pressure (CSP) independent of arterial pressure. We then perturbed CSP with random binary pressure sequences and identified the transfer function from CSP to arterial pressure. Shown in the left panels of Fig. 2 are the time series of CSP and aortic pressure. As can be seen, aortic pressure changes slowly toward the opposite direction in response to changes in CSP. This becomes even more evident in the transfer function (the right panel). The transfer function has low-pass filter characteristics. The phase response becomes nearly out-of-phase in the low frequency range suggesting the negative feedback nature of baroreflex system. Note that the magnitude squared coherence function is about 0.8 over the frequency range of interest. This is to say that most dominant characteristics of the total baroreflex open loop are captured by the linear transfer function.

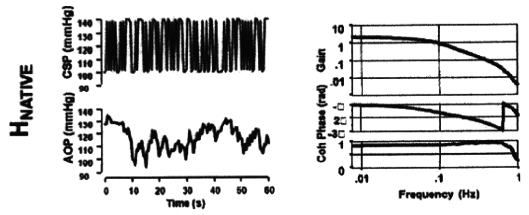

Fig. 2 Dynamic characteristics of native baroreflex system

In order to identify the actuator transfer function, we electrically stimulated the celiac ganglia with random binary pressure perturbations. Illustrated in the left panels of Fig. 3 are the time series of stimulation of celiac ganglia and aortic pressure responses. As can be seen, aortic pressure changes slowly toward the same direction in response to changes in stimulation. As anticipated the transfer function (the right panel) has low-pass filter characteristics. Unlike the total baroreflex loop, however, the phase response becomes nearly in-phase in the low frequency range. The magnitude squared coherence function is about 0.8 over the frequency range of interest. Again, it is reasonable to assume that most dominant characteristics of the actuator are captured by the linear transfer function.

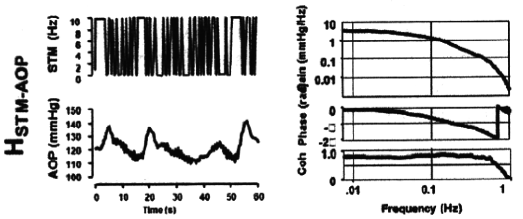

Fig. 3 Dynamic characteristics of sympathetic stimulation

We identified the transfer function (H_{BIONIC}) required for the controller by taking the ratio of H_{NATIVE} to $H_{STM-AOP}$. Since both dynamic characteristics of the total baroreflex loop and actuator are well represented by the linear transfer functions, the resultant H_{BIONIC} should reproduce the native characteristics of the baroreflex system when the feedback loop is closed. Shown in Fig. 4 are the changes in arterial pressure in response to orthostatic stresses under the open-loop baroreflex condition (baroreflex failure), the closed-loop baroreflex condition (native baroreflex) and the bionic baroreflex condition. Orthostatic stresses profoundly lowered arterial pressure in the absence of the native baroreflex. Closing the native baroreflex loop markedly attenuated the hypotensive responses. The activation of bionic baroreflex system also attenuated the hypotensive response as much as the native baroreflex system did. Statistical analysis indicated that the pressure regulation achieved by the bionic baroreflex system was indistinguishable from that achieved by the native baroreflex system.

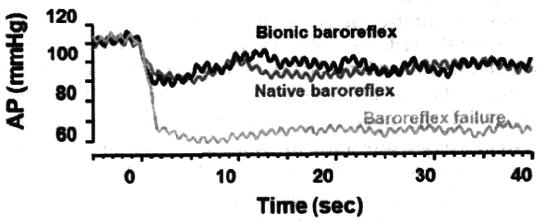

Fig. 4 Native baroreflex system vs. bionic baroreflex system

III. Discussion

We have shown that the bionic baroreflex system was as good as the native baroreflex system in regulating arterial pressure. The dynamic pressure responses to orthostatic stresses were indistinguishable between the native baroreflex system and the bionic baroreflex system. Although the baroreflex system is known to be nonlinear over the wide pressure range, we found that it is remarkably linear in the physiological pressure range. Because of this, the linear transfer function could represent the dominant characteristics of the baroreflex loop, and thereby allowed us to develop the bionic baroreflex system.

We can think of many anatomical sites where we can manipulate the activity of sympathetic system. In 1992, we stimulated the carotid sinus nerve to control the sympathetic system [1]. In 2004, we stimulated the spinal cord to stimulate the sympathetic efferent fibers [2]. The bionic mechanism worked beautifully regardless of the site of stimulation. It equally worked well in rats [3], rabbits [2], and dogs [1]. Although our experience of baroreflex failure in patients is limited, judging from its robustness, the bionic baroreflex system would work in patients as well [4]. If the bionic baroreflex system works in patients, it has a major impact as the treatment of baroreflex failure [5] that has been considered to be an incurable devastating disease.

IV. Conclusion

The bionic baroreflex system restores normal baroreflex function in an animal model of baroreflex failure.

ACKNOWLEDGMENT

This study was supported in part by Health and Labour Sciences Research Grant for Research on Medical Devices for Improving Impaired QOL from the Ministry of Health Labour and Welfare of Japan, Health and Labour Sciences Research Grant for Clinical Research from the Ministry of Health Labour and Welfare of Japan, and Grant-in-Aid for Scientific Research(S) (18100006) from the Japan Society for the Promotion of Science.

REFERENCES

[1] T. Kubota, H. Chishaki, T. Yoshida, K. Sunagawa, A. Takeshita, and Y. Nose, "How to encode arterial pressure into carotid sinus nerve to invoke natural baroreflex," *Am J Physiol* 263: H307-H313, 1992

[2] Y. Yanagiya, T. Sato, T. Kawada, M. Inagaki, T. Tatewaki, C. Zheng, A. Kamiya, H. Takaki, M. Sugimachi, and K. Sunagawa, "Bionic epidural stimulation restores arterial pressure regulation during orthostasis," *J Appl Physiol* 97: 984-990, 2004

[3] T. Sato, T. Kawada, T. Shishido, M. Sugimachi, and K. Sunagawa, "Novel therapeutic strategy against central baroreflex failure: A bionic baroreflex system," *Circulation* 100: 299-304, 1999

[4] F. Yamasaki, T. Ushida, T. Yokoyama, M. Ando, K. Yamasaki, and T. Sato, "Artificial baroreflex: clinical application of a bionic baroreflex system," *Circulation* 113: 634-639, 2008

[5] M. Sugimachi, and K. Sunagawa, "Bionic cardiology: exploration into a wealth of controllable body parts in the cardiovascular system," *IEEE Rev Biomed Eng.* 2: 172-186, 2009.

32nd Annual International Conference of the IEEE EMBS
Buenos Aires, Argentina, August 31 - September 4, 2010

Physiological Significance of Pressure-Volume Relationship: a Load-Independent Index and a Determinant of Pump Function

Masaru Sugimachi, *Member, IEEE*, Kenji Sunagawa, *Member, IEEE*,
Kazunori Uemura, and Toshiaki Shishido

Abstract—**Pressure-volume relationship permits conceptual integration with time-varying elastance, stress-strain relationship, and pressure-volume area. It has also superior usefulness to other indexes, both as a load-independent index of ventricular contractility and as a determinant of ventricular pump function.**

PRESSURE-VOLUME relationship has become a standard framework [1] for discussing the mechanical properties of the ventricles and sometimes atria. It has gained popularity because of its conceptual integration and its superior usefulness, both as a load-independent index and as a determinant of pump function. The concept of pressure-volume relationship agrees with to that of time-varying elastance, that of (time-varying) material properties of myocardium (i.e., stress-strain relationship), and that of pressure-volume area as the major determinant of myocardial oxygen consumption [2].

A. A Load-Independent Index

Pressure-volume relationship (PVR), especially the end-systolic pressure-volume relationship (ESPVR), has been repeatedly shown as one of the least load-sensitive index of ventricular contractility. Although preload-recruitable stroke work (PRSW) has been a rival, it is obvious that PRSW would no longer be load insensitive in extreme cases such as isovolumic beats.

Although detailed examination of ESPVR revealed its load-dependence (such as deactivation and activation associated with ejection) and curvilinearity [3], ESPVR is still the least load-dependent index of ventricular contractility. The apparent linearity of ESPVR seems to be observed just by chance, taking into consideration that ESPVR can be reconstructed from nonlinear (exponential) end-systolic stress-strain relationship of myocardium.

The most important advance what the concept of PVR has provided are the decoupling of heart from vasculature (preload and afterload), and the fact that actively contracting tissue would change its mechanical properties in cardiac cycles. Decoupling the heart enabled us to separately discuss the changes in the heart and the vasculature, rather than mix them and discuss only the measured hemodynamic variables. The uncovered complex load-dependence and curvilinearity would have not sacrificed the value of decoupling. The concept of changeable material property has simplified the explanation of complex time course of pressure development and ejection.

B. A Determinant of Pump Function

ESPVR has provided a method to precisely predict the stroke volume for given end-diastolic volume, heart rate and afterload resistance. This was accomplished by recoupling ESPVR with effective arterial elastance (mainly determined by heart rate and resistance). This is a major advantage over PRSW. What is more, even the pressure and flow waveform can be reconstructed by recoupling time-varying PVR (for the entire cardiac cycle) and arterial high-resolution impedance [4].

Manuscript received April 7, 2009. This work was supported in part by Grant-in-Aid for Scientific Research (B 20300164) from the Ministry of Education, Culture, Sports, Science and Technology, by Health and Labour Sciences Research Grants (H20-katsudo-shitei-007) from the Ministry of Health Labour and Welfare of Japan.

M. Sugimachi, K. Uemura, and T. Shishido are with the National Cardiovascular Center Research Institute, Suita, Osaka 5658565, Japan (corresponding author Masaru Sugimachi to provide phone: +81-6-6833 -5012; fax: +81-6-6835-5403; e-mail: su91mach@ri.ncvc.go.jp).

K. Sunagawa is with Kyushu University, Fukuoka 8128582 Japan. (e-mail: sunagawa@cardiol.med.kyushu-u.ac.jp).

REFERENCES

[1] K. Sagawa, L. Maughan, H. Suga, and K. Sunagawa, "Cardiac Contraction and the Pressure-Volume Relationship," New York, Oxford University Press, 1988.

[2] H. Suga, "Ventricular energetics," *Physiol. Rev.* vol. 70, no. 2, 247–277, Apr. 1990.

[3] D. Burkhoff, S. Sugiura, D. T. Yue, and K. Sagawa, "Contractility-dependent curvilinearity of end-systolic pressure-volume relations," *Am. J. Physiol.* vol. 252, no. 6, part 2, H1218–H1227, Jun. 1987.

[4] T. W. Latson, W. C. Hunter, D. Burkhoff, K. Sagawa, "Time sequential prediction of ventricular-vascular interactions," *Am. J. Physiol.* vol. 251, no. 6, part 2, H1341–H1353, Dec. 1986.

32nd Annual International Conference of the IEEE EMBS
Buenos Aires, Argentina, August 31 - September 4, 2010

Estimated Venous Return Surface and Cardiac Output Curve Precisely Predicts New Hemodynamics after Volume Change

Masaru Sugimachi, *Member, IEEE*, Kenji Sunagawa, *Member, IEEE*,
Kazunori Uemura, Atsunori Kamiya, Shuji Shimizu, Masashi Inagaki and Toshiaki Shishido

Abstract— **In our extended Guyton's model, the ability of heart to pump blood is characterized by a cardiac output curve and the ability of vasculature to pool blood by a venous return surface. These intersect in a three-dimensional coordinate system at the operating right atrial pressure, left atrial pressure, and cardiac output. The baseline cardiac output curve and venous return surface and their changes after volume change would predict new hemodynamics. The invasive methods needed to precisely characterize cardiac output curve and venous return surface led us to aim at estimating cardiac output curve and venous return surface from a single hemodynamic measurement. Using the average values for two logarithmic function parameters, and for two slopes of a surface, we were able to estimate cardiac output curve and venous return surface. The estimated curve and surface predicted new hemodynamics after volume change precisely.**

I. Introduction

OUR group has developed an extended Guyton's cardiovascular model, where the ability of the right- and left-sided heart to pump blood is integratively characterized by a single curve (cardiac output curve) and the ability of vasculature to pool blood is expressed as a surface (venous return surface). The cardiac output curve and the venous return surface intersect in a three-dimensional coordinate system, and the three coordinates show the operating right atrial pressure (RAP), left atrial pressure (LAP), and cardiac output (CO), respectively (Fig. 1).

If one knows the baseline cardiac output curve and venous return surface and how these change after volume infusion and depletion, one can predict new hemodynamics by combining a new cardiac output curve and a new venous return surface. The precise characterization of cardiac output curve and venous return surface, however, needs extremely invasive measures for changing loading conditions to be applicable to patients with heart diseases (see Sections IIB and IIC for the detailed invasive methods used in animal experiments). Therefore, the aim of this study was to circumvent this difficulty by establishing a method to approximately obtain the cardiac output curve and venous return surface from a single hemodynamic measurement.

Manuscript received April 7, 2009. This work was supported in part by Grant-in-Aid for Scientific Research (B 20300164, C 20500404) from the Ministry of Education, Culture, Sports, Science and Technology, by Health and Labour Sciences Research Grants (H20-katsudo-shitei-007) from the Ministry of Health Labour and Welfare of Japan.

M. Sugimachi, K. Uemura, A. Kamiya, S. Shimizu, M. Inagaki and T. Shishido are with the National Cardiovascular Center Research Institute, Suita, Osaka 5658565, Japan (corresponding author Masaru Sugimachi to provide phone: +81-6-6833-5012; fax: +81-6-6835-5403; e-mail: su91mach@ri.ncvc.go.jp).

K. Sunagawa is with Kyushu University, Fukuoka 8128582 Japan. (e-mail: sunagawa@cardiol.med.kyushu-u.ac.jp).

II. Model and Methods

A. Extended Guyton's Model

We have extended Guyton's model [1] to handle a number of difficulties frequently encountered in clinical settings in patients with predominantly unilateral heart failure.

First, we extended a 2D (RAP-CO) Guyton's model to a 3D (RAP-LAP-CO) model, and introduced a third axis for LAP (Fig. 1) [2], [3]. By this modification, we can get the operating LAP directly from the intersection between cardiac output curve and venous return surface. LAP indicates the degree of pulmonary congestion and inadequate blood oxygenation, and normal range of LAP is as important as that of cardiac output and that of blood pressure for sustaining life.

Second, in this 3D model, we can separately express the changes in pumping ability of the right- and left-sided heart; the 3D cardiac output curve (Fig. 1, thick curve) is, in reality, the integration of two separate 2D cardiac output curves. The pumping ability of the right-sided heart can be obtained by projecting the 3D curve to the RAP-CO plane, and that of the

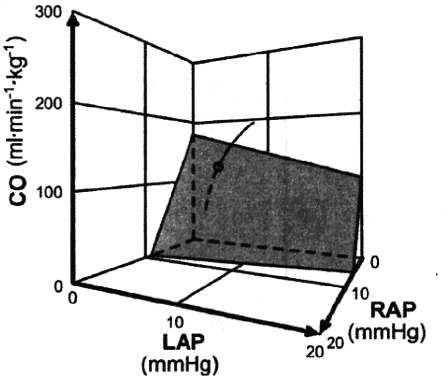

Fig. 1. An extended Guyton's model. The curve integratively expresses the pumping ability of right- and left-sided heart. The shaded surface characterizes the blood-pooling ability of the vasculature. RAP, right atrial pressure; LAP, left atrial pressure; CO, cardiac output (per kg of body weight).

left-sided heart can be obtained by projecting it to the LAP-CO plane. The preferential decrease in the pumping ability of the left-sided heart, such as seen in the ischemic heart disease, would rotate the projected curve to the RAP-LAP plane to the direction of LAP axis.

Third, the blood-pooling ability of the vasculature and the effect of stressed blood on the vasculature can be expressed by the venous return surface (Fig. 1, shaded surface). This surface remains the same so long as the total stressed volume is unchanged irrespective of its distribution. Increased LAP and pulmonary congestion associated with left-sided heart failure is characterized by blood redistribution from systemic to pulmonary vascular beds. Blood redistribution, however, would not change the venous return surface itself (i.e., unaffected by the changes in pumping ability). This is in sharp contrast with the classical venous return curve of Guyton's model. The relatively flat slope of the surface to the direction of LAP axis indicates the smaller blood-pooling ability of pulmonary vascular beds. As a result, the decrease in RAP with systemic-to-pulmonary blood redistribution is much smaller than the increase in LAP. This is shown, also illustratively in Fig. 1, by moving along the venous return surface and parallel to the RAP-LAP plane (keeping CO constant).

B. Animal Experiments to Characterize Cardiac Output Curve

We planned to characterize both cardiac output curve and venous return surface as precisely as possible in animals by using even the most invasive methods. In characterizing the pumping ability, only the heart of animals is needed; in characterizing the blood-pooling ability, only the vasculature of animals is needed.

The experiment for the characterization of cardiac output curve was less invasive. We do not need to physically detach the vasculature from the heart. Rather, in 7 dogs, by withdrawing and transfusing blood in a stepwise manner, we were able to obtain both right- and left-sided cardiac output curve simultaneously.

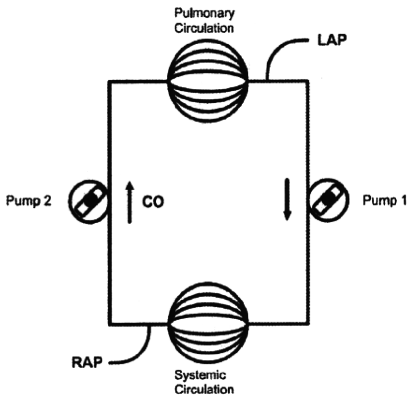

Fig. 2. An experimental scheme to characterize venous return surface. By replacing the right- and the left-sided heart with respective roller pumps, one can change cardiac output of the right- and the left-sided heart independently.

C. Animal Experiments to Characterize Venous Return Surface

Figure 2 depicts the scheme of an experiment to characterize the venous return surface. To extract only the vasculature and to physically remove the animal heart from the cardiovascular system, we replaced the right- and the left-sided heart with respective roller pumps. These pumps allow us to change CO of the right- and left-sided heart independently. Changing the flow of the two pumps at the same level would simulate the weak or strong heart. Transient unbalancing flow would redistribute blood between systemic and pulmonary vascular beds.

In each of 6 canine preparations, we obtained 6 different hemodynamic (CO, RAP, LAP) data sets. In each animal, these sets of data were fit to a flat surface in 3D coordinate system by linear regression analysis. CO was selected as a dependent variable and RAP (~2-5 mmHg) and LAP (~0-10 mmHg) are selected as independent variables.

D. Method to Estimate Cardiac Output Curve from a Single Hemodynamic Data Set

We fit experimental data to two logarithmic curves (one for the right- and the other for the left-sided heart), based on the knowledge of exponential end-diastolic pressure volume relationship and linear end-systolic pressure volume relationship, as follows.

$$CO = S\,[\ln(P - A) + B]$$

Here, P indicates RAP or LAP; A, B, and S are parameters. As analytical solution indicated that A and B is only dependent on diastolic properties of the ventricles, and is unlikely to change acutely, we fixed these parameters as their respective average values. This enabled one to estimate cardiac output curve from a single hemodynamic data set.

E. Method to Estimate Venous Return Surface from a Single Hemodynamic Data Set

We were able to fit experimental data to a flat surface well (r^2=0.92 to 0.99). As the surfaces from 6 animals were reasonably parallel (see Results), we used average slopes to estimate venous return surface from a single hemodynamic data set. Furthermore, as CO-axis intercept was linearly related to the withdrawn or transfused blood volume, we used this relationship to estimate a new venous return surface after blood volume change.

III. Results

A. Method to Estimate Cardiac Output Curve from a Single Hemodynamic Data Set

We were able to fit the cardiac output curve of both the right- and the left-sided heart by logarithmic functions (right-sided heart, r^2=0.90 to 0.99; left-sided heart, r^2=0.95 to 0.99). Since standard deviation of parameter A (1.29) or that of parameter

B (1.25) was much smaller than that of parameter S (30.9), we used the respective average values for A and B. The obtained cardiac output curves for right- and left-sided heart were as follows.

$$CO = S_R [\ln(RAP - 2.13) + 1.90] \quad (1)$$

$$CO = S_L [\ln(LAP - 2.03) + 0.80] \quad (2)$$

Parameters S_R and S_L can be used to represent the magnitude of the pumping ability of the right- and left-sided heart, respectively. As S_R and S_L can be calculated from a single set of hemodynamic data, we can approximately get cardiac output curve.

B. Method to Estimate Cardiac Output Curve from a Single Hemodynamic Data Set

In Figure 3 we have shown the venous return surfaces obtained from all 6 dogs. The surfaces were shown (as if they were lines) from the direction parallel to the surface. The figure indicates that in each of 6 dogs, all 6 data sets are located very near the flat surface. This implied the goodness of the fit of these data points to the flat surface. It is also shown that three coordinate axes are almost parallel among these dogs. This is because the slopes of the surface were almost the same among animals. These experimental results indicated that the venous return surface is linear and can be expressed by a common equation for all animals.

$$CO = CO_{max} - 19.61\ RAP - 3.49\ LAP.$$

Further, by infusing or withdrawing known amounts of blood, we were able to relate CO_{max} to blood volume as

$$CO_{max} = V / 0.129 \quad (3)$$

where V is total intravascular stressed blood volume. Combining these equations resulted in

$$CO = V / 0.129 - 19.61\ RAP - 3.49\ LAP. \quad (4)$$

Parameter V can be used to monitor the changes in total stressed blood volume. As V can be calculated from a single set of hemodynamic data, we can approximately get venous return surface.

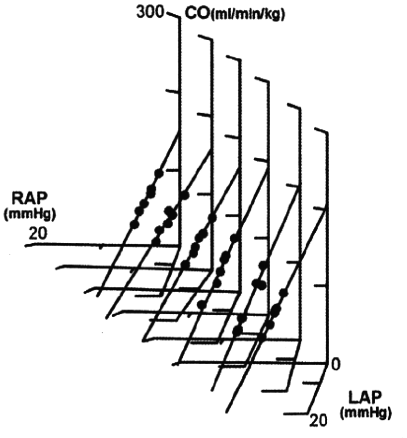

Fig. 3. Venous return surfaces obtained from 6 dogs. For each dog, the venous return surface was projected in a direction parallel to the surface, and was superimposed with each other.

C. Prediction of New Hemodynamics after Volume Change

We predicted new hemodynamics after volume change as follows. First, baseline cardiac output curve (Equations 1 and 2) and venous return surface (Equation 4) were approximately estimated from a single baseline hemodynamic data, by the methods shown in two previous sections IIIA and IIIB. Next, a new venous return surface was estimated by changing CO_{max} according to Equation 3. We assumed that cardiac output curve would not change by the volume change. Finally, new hemodynamics data were estimated by calculating the intersection between cardiac output curve and venous return surface.

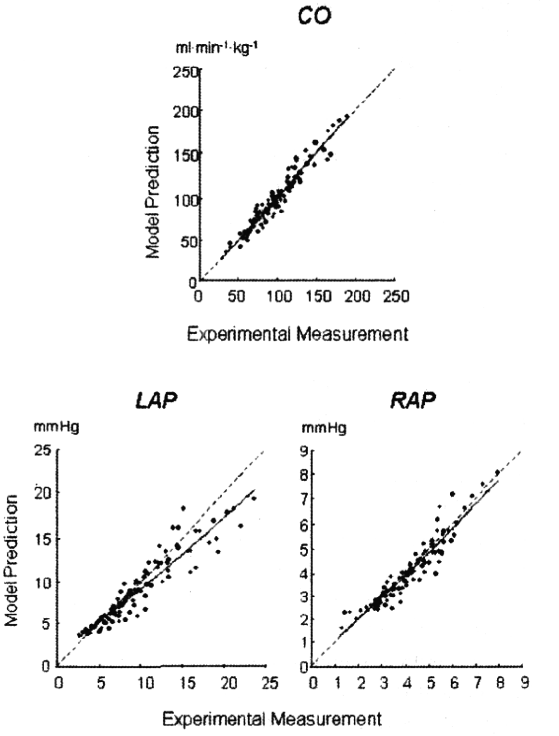

Fig. 4. Prediction of CO, LAP, and RAP from estimated cardiac output curve and venous return surface after volume change.

Using these new estimated cardiac output curve and venous return surface, we were able to predict the hemodynamics (y value) after withdrawal or transfusion of blood of known volume precisely as compared to actually measured (x value) (CO: $y = 0.93x + 6.5$, $r^2 = 0.96$, SEE [standard error of estimate] = 7.5 $ml \cdot min^{-1} \cdot kg^{-1}$; LAP: $y = 0.90x + 0.5$, $r^2 = 0.93$, SEE = 1.4 mmHg; RAP: $y = 0.87x + 0.4$, $r^2 = 0.91$, SEE = 0.4 mmHg) (Fig. 4) [3].

IV. Discussion

A. Most Undiagnosed Property: Total Stressed Blood Volume

The three major players of the cardiovascular system are heart

(pumps), vasculature (tubes with resistive and capacitive function), and blood. These three components interactively determine all hemodynamic variables. Of these, pump function and resistive function of vasculature have been repeatedly evaluated in previous studies. These properties were also evaluated clinically.

In contrast, evaluation of the vascular capacitive function and that of the blood volume have been relatively ignored. Even though blood volume drastically changes, there have been no reasonable methods to evaluate total stressed blood volume precisely. Simple measurement of central venous pressure (i.e., RAP) cannot be a proxy marker of blood volume, as this pressure value also changes with pump function or with redistribution of blood.

It is clear from our results [$V = (CO + 19.61\ RAP + 3.49\ LAP) \times 0.129$] that blood volume (V) is not solely determined by RAP. Rather, all three variables CO, RAP and LAP contribute (not as differently as have been considered) to the changes in blood volume. Clinicians should know that when LAP increases by 5.6 mmHg, or CO increases by 0.98L/min in 50-Kg patients, similar blood volume increases as RAP is increased by 1 mmHg.

Implantable devices with volume monitoring functionality for patients with heart failure should also take these results into consideration.

B. Hemodynamic Variables and Cardiovascular Properties

In clinical practice, physicians have to restore hemodynamic variables to their respective normal range. Of these, the most important three variables include blood pressure, CO and LAP. These variables are essentially important as blood pressure determines the perfusion of vital organs (for short-term need), CO determines the perfusion of peripheral tissues (for long-term need), and LAP determines blood oxygenation in lungs.

These hemodynamic variables are, in turn, determined by the interaction between cardiovascular properties, such as pump, resistance, capacitance, and blood volume. What clinicians should know, monitor, and correct are in reality these cardiovascular properties. Most drugs and interventions are aimed at correcting mainly one of these properties. From these viewpoints, the method to continuously estimate cardiovascular properties from measured hemodynamics is the most basic need in patient monitoring.

V. CONCLUSION

We have successfully developed a method to estimate the cardiac output curve and venous return surface from a single hemodynamic data set. This method enabled to predict new hemodynamics after withdrawal or transfusion of blood of known volume.

REFERENCES

[1] A. C. Guyton, "Determination of cardiac output by equating venous return curves with cardiac response curves," *Physiol. Rev.* vol. 35, no. 1,123–129, Jan. 1955.

[2] K. Uemura, M. Sugimachi, T. Kawada, A. Kamiya, Y. Jin, *et al.*, "A novel framework of circulatory equilibrium," *Am. J. Physiol. Heart Circ. Physiol.* vol. 286, no. 6, pp. H2376–H2385, Jun. 2004.

[3] K. Uemura, T. Kawada, A. Kamiya, T. Aiba, I. Hidaka, *et al.*, "Prediction of circulatory equilibrium in response to changes in stressed blood volume," *Am. J. Physiol. Heart Circ. Physiol.* vol. 289, no. 1, H301–H307, Jul. 2005.

Am J Physiol Regul Integr Comp Physiol 300: R155–R165, 2011.
First published November 3, 2010; doi:10.1152/ajpregu.00540.2010.

Dynamic characteristics of baroreflex neural and peripheral arcs are preserved in spontaneously hypertensive rats

Toru Kawada,[1] Shuji Shimizu,[1,2] Atsunori Kamiya,[1] Yusuke Sata,[1] Kazunori Uemura,[1] and Masaru Sugimachi[1]

[1]*Department of Cardiovascular Dynamics, National Cerebral and Cardiovascular Center Research Institute, Osaka, Japan; and* [2]*Japan Association for the Advancement of Medical Equipment, Tokyo, Japan*

Submitted 18 August 2010; accepted in final form 3 November 2010

Kawada T, Shimizu S, Kamiya A, Sata Y, Uemura K, Sugimachi M. Dynamic characteristics of baroreflex neural and peripheral arcs are preserved in spontaneously hypertensive rats. *Am J Physiol Regul Integr Comp Physiol* 300: R155–R165, 2011. First published November 3, 2010; doi:10.1152/ajpregu.00540.2010.—Although baroreceptors are known to reset to operate in a higher pressure range in spontaneously hypertensive rats (SHR), the total profile of dynamic arterial pressure (AP) regulation remains to be clarified. We estimated open-loop transfer functions of the carotid sinus baroreflex in SHR and Wistar Kyoto (WKY) rats. Mean input pressures were set at 120 (WKY_{120} and SHR_{120}) and 160 mmHg (SHR_{160}). The neural arc transfer function from carotid sinus pressure to efferent splanchnic sympathetic nerve activity (SNA) revealed derivative characteristics in both WKY and SHR. The slope of dynamic gain (in decibels per decade) between 0.1 and 1 Hz was not different between WKY_{120} (10.1 ± 1.0) and SHR_{120} (10.4 ± 1.1) but was significantly greater in SHR_{160} (13.2 ± 0.8, $P < 0.05$ with Bonferroni correction) than in SHR_{120}. The peripheral arc transfer function from SNA to AP showed low-pass characteristics. The slope of dynamic gain (in decibels per decade) did not differ between WKY_{120} (−34.0 ± 1.2) and SHR_{120} (−31.4 ± 1.0) or between SHR_{120} and SHR_{160} (−32.8 ± 1.3). The total baroreflex showed low-pass characteristics and the dynamic gain at 0.01 Hz did not differ between WKY_{120} (0.91 ± 0.08) and SHR_{120} (0.84 ± 0.13) or between SHR_{120} and SHR_{160} (0.83 ± 0.11). In both WKY and SHR, the declining slope of dynamic gain was significantly gentler for the total baroreflex than for the peripheral arc, suggesting improved dynamic AP response in the total baroreflex. In conclusion, the dynamic characteristics of AP regulation by the carotid sinus baroreflex were well preserved in SHR despite significantly higher mean AP.

systems analysis; transfer function; white noise; sympathetic nerve activity; arterial pressure

THE ARTERIAL BAROREFLEX IS an important negative feedback system that stabilizes systemic arterial pressure (AP) against exogenous disturbances in daily activities. The sympathetic limb of the arterial baroreflex system may be analyzed by dividing it into two principal subsystems (23). One is a controller subsystem that describes the relationship between baroreceptor pressure input and efferent sympathetic nerve activity (SNA). The other is an effector subsystem that describes the relationship between SNA and AP. Hereafter, in this article, we refer to the former as the neural arc and the latter as the peripheral arc (9). In normal physiological conditions, changes in AP affect SNA via the neural arc, and the changes in SNA, in turn, affect AP via the peripheral arc. This closed-loop operation makes it difficult to identify the dynamic characteristics of the neural and peripheral arcs separately (see APPENDIX) (18). To circumvent the closed-loop problem, the carotid sinus baroreceptor regions were isolated from the systemic circulation, and open-loop transfer function analyses were performed in anesthetized rabbits (9) and rats (31). In both species, the neural arc revealed "derivative" characteristics, which means that the dynamic gain of the SNA response becomes greater as the frequency of modulation increases. In contrast, the peripheral arc showed "low-pass" characteristics, which means that the dynamic gain of the AP response becomes smaller as the frequency of modulation increases. It has been interpreted that the fast neural arc partially compensates for the slow peripheral arc to improve the speed of response of the total baroreflex system (9).

In chronic hypertension, the arterial baroreflex is reset to operate in a higher pressure range (2). Both carotid sinus (24) and aortic baroreceptors (30) show the resetting in spontaneously hypertensive rats (SHR). Although changes in vascular properties induced by sustained hypertension, such as reduced distensibility, may decrease the baroreflex sensitivity, the dynamic characteristics of AP regulation by the arterial baroreflex in hypertension are not fully understood. In a previous study, Harada et al. (7) have shown that the baroreflex neural arc retains its derivative characteristics in SHR. Since they perturbed AP by aortic balloon inflation and deflation, they were unable to quantify the dynamic AP response to changes in SNA (i.e., the peripheral arc). As a result, the total profile of the dynamic AP regulation in SHR remains to be clarified. The aim of the present study was to comprehensively identify the dynamic characteristics of the neural arc, peripheral arc, and total baroreflex in SHR and compare them with those estimated in normotensive Wistar Kyoto rats (WKY).

MATERIALS AND METHODS

Animals were cared for in strict accordance with the Guiding Principles for the Care and Use of Animals in the Field of Physiological Sciences, which has been approved by the Physiological Society of Japan. All experimental protocols were reviewed and approved by the Animal Subjects Committee at the National Cerebral and Cardiovascular Center.

Surgical preparation. Main experiments were performed in age-matched male WKY ($n = 7$, 21.6 ± 3.7 wk) and SHR ($n = 6$, 22.2 ± 4.5 wk). Each rat was anesthetized with an intraperitoneal injection (2 ml/kg) of a mixture of urethane (250 mg/ml) and α-chloralose (40 mg/ml), and mechanically ventilated with oxygen-enriched room air. A venous catheter was inserted into the right femoral vein, and the above anesthetic mixture, diluted 20-fold, was administered continuously (2–3 $ml \cdot kg^{-1} \cdot h^{-1}$). An arterial catheter was inserted into the right femoral artery to measure AP. Heart rate (HR) was obtained

Address for reprint requests and other correspondence: T. Kawada, Dept. of Cardiovascular Dynamics, National Cerebral and Cardiovascular Center Research Institute, 5–7-1 Fujishirodai, Suita, Osaka 565–8565, Japan (e-mail: torukawa@res.ncvc.go.jp).

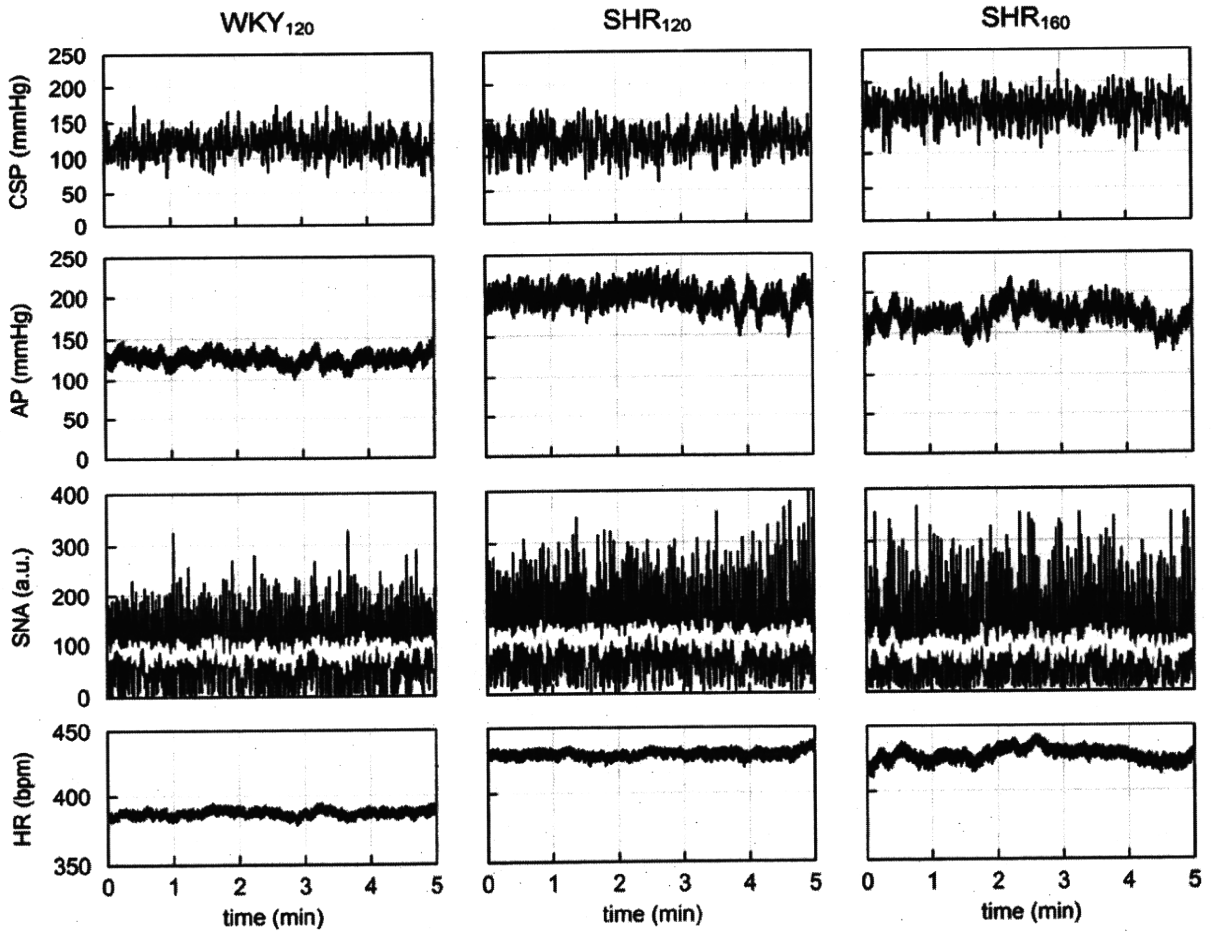

Fig. 1. Typical recordings of carotid sinus pressure (CSP), arterial pressure (AP), sympathetic nerve activity (SNA), and heart rate (HR) obtained from a Wistar Kyoto (WKY) rat and a spontaneously hypertensive rat (SHR). CSP was perturbed according to a Gaussian white noise with mean input pressure of 120 mmHg (WKY_{120} and SHR_{120}) or 160 mmHg (SHR_{160}). White lines in the SNA data indicate 2-s moving average SNA signals.

from AP through a cardiotachometer. Another venous catheter was inserted into the left femoral vein to infuse Ringer solution (6 $ml \cdot kg^{-1} \cdot h^{-1}$).

A postganglionic branch from the splanchnic sympathetic nerve was exposed through a left flank incision and a pair of stainless-steel wire electrodes (Bioflex wire AS633; Cooner Wire, Chatsworth, CA) was attached to record SNA. The nerve and electrodes were covered with silicone glue (Kwik-Sil; World Precision Instruments, Sarasota, FL, USA) for insulation and fixation. To quantify the nerve activity, the preamplified nerve signal was band-pass filtered at 150–1,000 Hz, and then full-wave rectified and low-pass filtered with a cut-off frequency of 30 Hz. Pancuronium bromide (0.4 $mg \cdot kg^{-1} \cdot h^{-1}$) was administered to prevent muscular activity from contaminating the SNA recording. At the end of the experiment, we confirmed the disappearance of SNA after an intravenous bolus injection of a ganglionic blocker hexamethonium bromide (60 mg/kg) and recorded the noise level.

Table 1. *Mean arterial pressure, heart rate, and sympathetic nerve activity during dynamic input protocol*

	WKY_{120}	SHR_{120}	SHR_{160}
Mean AP, mmHg	105 ± 5	176 ± 17**	143 ± 14†
Mean HR, bpm	406 ± 18	432 ± 19	423 ± 15
Mean SNA, au	85 ± 12	147 ± 15*	110 ± 15†

Data are presented in means ± SE values [$n = 7$ for Wistar-Kyoto (WKY) and $n = 6$ for spontaneously hypertensive rats (SHR)]. AP, arterial pressure; HR, heart rate; SNA, sympathetic nerve activity; bpm, beats per minute; au, arbitrary unit. *$P < 0.05$ and **$P < 0.01$, WKY_{120} vs. SHR_{120} by unpaired-t-test with Bonferroni correction. †$P < 0.05$, SHR_{120} vs. SHR_{160} by paired-t-test with Bonferroni correction.

Bilateral vagal and aortic depressor nerves were sectioned at the neck to avoid reflexes from the cardiopulmonary region and aortic arch. The carotid sinus regions were isolated from the systemic circulation using previously reported procedures (32, 34) with modifications. Briefly, a 7–0 polypropylene suture with a fine needle (PROLENE; Ethicon, Cornelia, GA) was passed through the tissue between the external and internal carotid arteries, and the external carotid artery was ligated close to the carotid bifurcation. The internal carotid artery was embolized by injecting two to three steel balls (0.8 mm in diameter; Tsubaki Nakashima, Nara, Japan) from the common carotid artery. The isolated carotid sinuses were filled with warmed Ringer solution through catheters inserted into the common carotid arteries. The carotid sinus pressure (CSP) was controlled using a servo-controlled piston pump. Heparin sodium (100 U/kg) was given intravenously to prevent blood coagulation. Body temperature was maintained at ~38°C with a heating pad.

Protocols. Some animals showed deterioration of baroreflex responses soon after the completion of the surgical preparation, possibly due to the surgical damage to the carotid sinus nerves or the low brain

perfusion after bilateral common carotid occlusion. The baroreflex study described below was conducted only in animals showing persistent baroreflex-mediated SNA, AP, and HR responses for more than 30 min after completion of the surgical preparation.

To estimate dynamic characteristics of the carotid sinus baroreflex, CSP was perturbed for 20 min using a Gaussian white noise (GWN) signal with a standard deviation of 20 mmHg (11, 12). The whiteness of the input is essential to estimate the system characteristics stably over a frequency range of interest (see APPENDIX). The mean input CSP was set at 120 mmHg in WKY (WKY_{120}) and SHR (SHR_{120}). Taking into account a priori knowledge that the baroreceptor is reset to a higher pressure range in SHR (2, 24), the same rats in SHR_{120} were also tested at a mean input CSP of 160 mmHg (SHR_{160}). The switching interval of GWN was 500 ms. The resulting input power spectral density was relatively constant up to 1 Hz, which was expected to cover the upper frequency range of interest with respect to the sympathetic arterial baroreflex in rats (31).

A supplemental protocol was performed in an additional three 18-wk-old male WKY rats to test the effect of changing the mean input CSP on the transfer function estimation. The GWN input was applied with the mean CSP set at 120 mmHg ($WKY_{120\text{-}S}$) and 160 mmHg ($WKY_{160\text{-}S}$). Six data sets were analyzed by acquiring two data sets from each rat using GWN signals of different sequences.

Data analysis. Data were sampled at 200 Hz using a 16-bit analog-to-digital converter and stored in a dedicated laboratory computer system. Dynamic characteristics of the baroreflex neural arc, peripheral arc, total baroreflex, and HR control were estimated by a standard open-loop transfer function analysis (see APPENDIX) (20). Data analysis was started from 120 s after initiation of the GWN input. The input-output data pairs were resampled at 10 Hz, and 12 segments were processed using 50%-overlapping bins of 1,024 points each.

To facilitate understanding of the transfer function, the step response corresponding to the transfer function was calculated as follows. A system impulse response was derived from the inverse Fourier transform of the transfer function. The step response was then obtained from the time integral of the impulse response.

Because the magnitude of SNA varied among animals depending on the recording conditions, SNA was normalized in each animal by assigning unity to the mean dynamic gain for frequencies below 0.03 Hz in the neural arc transfer function, for WKY_{120} and SHR_{120}. The following parameters of the transfer functions were compared: dynamic gain values at 0.01, 0.1, and 1 Hz ($G_{0.01}$, $G_{0.1}$, and G_1), and the slope of dynamic gain (G_{slope}) for the frequency range of 0.1 to 1 Hz. G_{slope} was calculated by a regression analysis between log frequency and log dynamic gain. For step response analysis of the neural arc, the negative peak response (S_{peak}), time to the negative peak (T_{peak}), and step response at 10 s (S_{10}) were calculated. For step response analyses of the peripheral arc, total baroreflex, and HR control, the steady-state response at 50 s (S_{50}) and initial slope (S_{slope}) were calculated. To calculate S_{slope}, a threshold value was determined at 5% S_{50}, and the

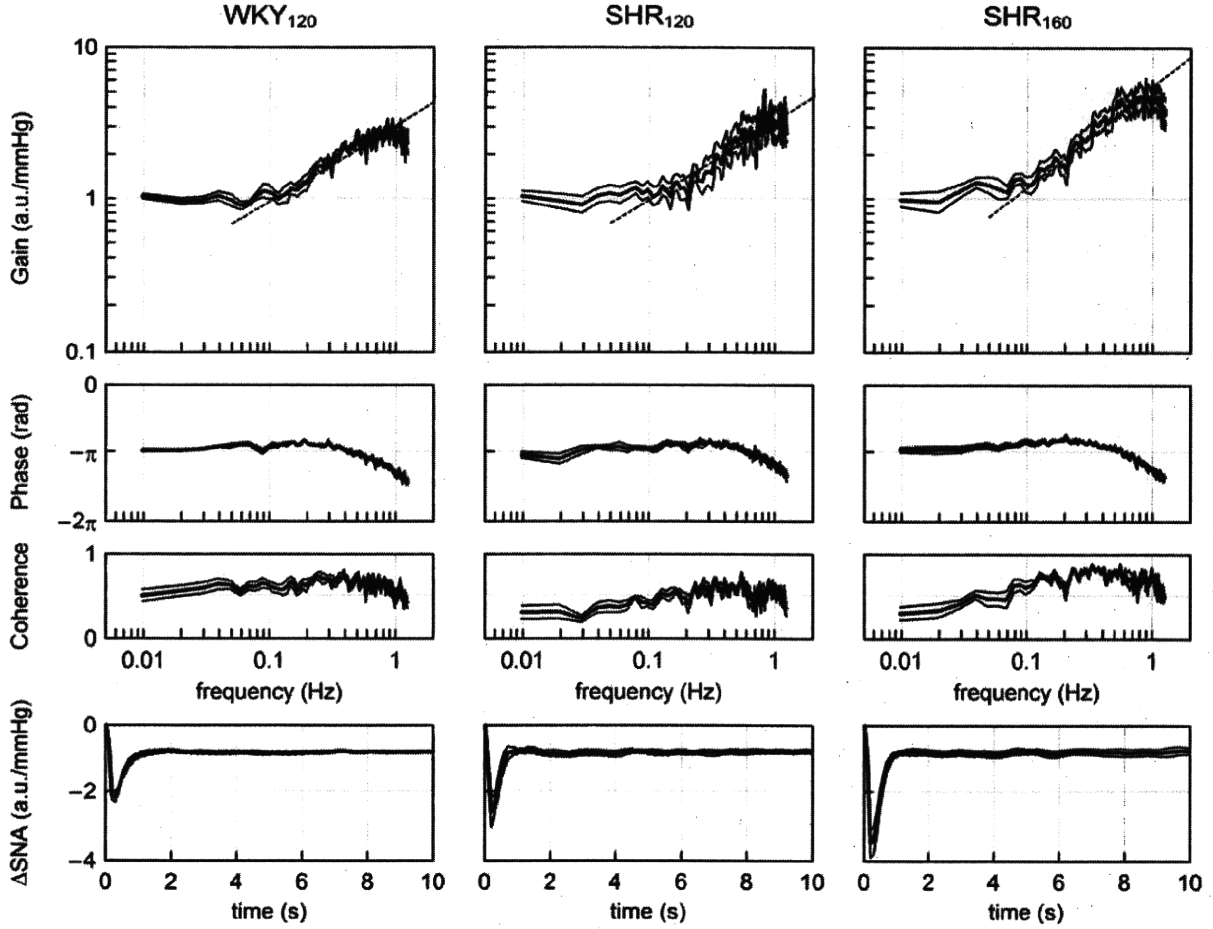

Fig. 2. Transfer functions of the baroreflex neural arc from CSP to SNA averaged for WKY_{120}, SHR_{120}, and SHR_{160} groups. Gain, phase, and coherence plots are shown. In the gain plots, the dashed oblique line indicates the mean slope of the dynamic gain (G_{slope}) estimated in the frequency range from 0.1 to 1 Hz. G_{slope} is significantly steeper in SHR_{160} than in SHR_{120}. *Bottom*: step responses of SNA calculated from the corresponding neural arc transfer functions. The peak response (S_{peak}) is significantly more negative in SHR_{160} than in SHR_{120}. In all panels, the bold and thin lines indicate mean and mean ± SE values, respectively.

first data point that exceeded the threshold was obtained. Starting from this first data point, a regression analysis was repeated while increasing the number of data points for the regression. The steepest slope thus obtained was defined as S_{slope}.

Statistical analysis. All data are presented as means ± SE. Differences between WKY_{120} and SHR_{120} were tested using unpaired *t*-test. Differences between SHR_{120} and SHR_{160} were tested using paired *t*-test. Taking into account the duplicated comparisons of the SHR_{120} data, differences between groups were considered to be significant when $P < 0.05$ with Bonferroni correction (i.e., $P < 0.025$ and $P < 0.005$ were interpreted as $P < 0.05$ and $P < 0.01$, respectively) (5). In the supplemental protocol, parameters were compared between $WKY_{120\text{-}S}$ and $WKY_{160\text{-}S}$ using paired *t*-test.

RESULTS

Figure 1 shows the typical experimental data obtained from an individual rat in the WKY_{120}, SHR_{120}, and SHR_{160} groups. The SHR_{120} and SHR_{160} data were derived from the same animal. In each group, CSP was perturbed according to a GWN signal, which caused variations in AP, SNA, and HR. The mean AP was significantly higher in SHR_{120} than in WKY_{120}, confirming hypertension in SHR (Table 1). The mean AP was significantly lower in SHR_{160} than in SHR_{120}, indicating that increasing the mean CSP enabled the reduction of the mean AP in SHR. The white lines in the SNA plots indicate 2-s moving average signals. Although mean SNA was higher in SHR_{120} than in WKY_{120}, this comparison could be influenced by the normalization of SNA. The mean SNA in SHR_{160} decreased significantly to 74 ± 6% of that in SHR_{120}. Although changes in mean HR appeared to parallel the changes in mean AP, there were no significant changes across the groups (Table 1).

The neural arc transfer functions averaged from the WKY_{120}, SHR_{120}, and SHR_{160} groups are shown in Fig. 2. In the gain plots, $G_{0.01}$ approximated unity in WKY_{120} and SHR_{120} because of the normalization procedure (Table 2). The dynamic gain became greater as the frequency increased above 0.1 Hz. There were no significant differences in $G_{0.1}$, G_1, and G_{slope} between WKY_{120} and SHR_{120}. $G_{0.01}$ also approximated unity in SHR_{160}, although SNA was normalized by the same normalization factor used for the SHR_{120} data. While $G_{0.1}$ did not differ significantly between SHR_{120} and SHR_{160}, G_1 and G_{slope} were significantly greater in SHR_{160}. The phase plots of three groups were similar: the phase was close to $-\pi$ radians at 0.01 Hz, deviated slightly toward 0 radians until 0.5 Hz, and then delayed beyond $-\pi$ radians as the frequency increased above 0.7 Hz. For the step responses, S_{10} and T_{peak} did not differ between WKY_{120} and SHR_{120} or between SHR_{120} and SHR_{160}. S_{peak} was not significantly different between WKY_{120} and SHR_{120} but was significantly more negative in SHR_{160} than in SHR_{120}.

The peripheral arc transfer functions averaged from the WKY_{120}, SHR_{120}, and SHR_{160} groups are shown in Fig. 3. In the gain plots, the dynamic gain became smaller, as the frequency increased above 0.05 Hz. $G_{0.01}$, $G_{0.1}$, G_1, and G_{slope} did not differ significantly between WKY_{120} and SHR_{120} or between SHR_{120} and SHR_{160} (Table 2). The phase plots of three groups were similar: the phase approached 0 radians at 0.01 Hz and was delayed by -2π radians as the frequency increased to 1 Hz. For the step responses, S_{50} and S_{slope} did not differ between WKY_{120} and SHR_{120} or between SHR_{120} and SHR_{160}.

Table 2. *Parameters of estimated transfer functions and step responses*

	WKY_{120}	SHR_{120}	SHR_{160}
Neural arc			
$G_{0.01}$, au/mmHg	1.04 ± 0.04	1.06 ± 0.08	1.01 ± 0.11
$G_{0.1}$, au/mmHg	1.15 ± 0.11	1.16 ± 0.14	1.35 ± 0.13
G_1, au/mmHg	2.73 ± 0.21	3.41 ± 0.51	4.84 ± 0.64††
G_{slope}, dB/decade	10.1 ± 1.0	10.4 ± 1.1	13.2 ± 0.8†
S_{10}, au/mmHg	−0.81 ± 0.03	−0.79 ± 0.05	−0.79 ± 0.11
S_{peak}, au/mmHg	−2.22 ± 0.15	−2.71 ± 0.35	−3.60 ± 0.40††
T_{peak}, s	0.37 ± 0.03	0.33 ± 0.02	0.35 ± 0.02
Peripheral arc			
$G_{0.01}$, mmHg/au	0.75 ± 0.07	0.79 ± 0.14	0.79 ± 0.14
$G_{0.1}$, mmHg/au	0.35 ± 0.05	0.48 ± 0.14	0.45 ± 0.12
G_1, mmHg/au	0.014 ± 0.008	0.008 ± 0.002	0.008 ± 0.003
G_{slope}, dB/decade	−34.0 ± 1.2	−31.4 ± 1.0	−32.8 ± 1.3
S_{50}, mmHg/au	0.89 ± 0.06	0.85 ± 0.15	0.81 ± 0.15
S_{slope}, mmHg·au^{-1}·s^{-1}	0.14 ± 0.01	0.20 ± 0.05	0.18 ± 0.05
Total baroreflex			
$G_{0.01}$, mmHg/mmHg	0.91 ± 0.08	0.84 ± 0.13	0.83 ± 0.11
$G_{0.1}$, mmHg/mmHg	0.41 ± 0.06	0.53 ± 0.09	0.58 ± 0.10
G_1, mmHg/mmHg	0.023 ± 0.009	0.025 ± 0.005	0.034 ± 0.006
G_{slope}, dB/decade	−24.6 ± 1.3‡‡	−22.3 ± 1.3‡‡	−19.8 ± 1.3‡‡
S_{50}, mmHg/mmHg	−1.03 ± 0.10	−0.85 ± 0.08	−0.83 ± 0.08
S_{slope}, mmHg·mmHg^{-1}·s^{-1}	−0.20 ± 0.02	−0.28 ± 0.04	−0.32 ± 0.05
HR control			
$G_{0.01}$, bpm/mmHg	0.46 ± 0.05	0.22 ± 0.04**	0.27 ± 0.05
$G_{0.1}$, bpm/mmHg	0.11 ± 0.01	0.04 ± 0.01**	0.08 ± 0.02†
S_{50}, bpm/mmHg	−0.52 ± 0.07	−0.18 ± 0.04**	−0.23 ± 0.05
S_{slope}, bpm·mmHg^{-1}·s^{-1}	−0.050 ± 0.004	−0.025 ± 0.005**	−0.036 ± 0.009

Data are presented as means ± SE ($n = 7$ for WKY and $n = 6$ for SHR). $G_{0.01}$, $G_{0.1}$, and G_1, dynamic gain values at 0.01, 0.1, and 1 Hz, respectively; G_{slope}, slope of dynamic gain between 0.1 and 1 Hz; S_{50}, steady-state response at 50 s; S_{peak}, peak response; S_{slope}, initial slope; S_{10}, step response at 10 s; T_{peak}, time to the negative peak. **$P < 0.01$ WKY_{120} vs. SHR_{120} by unpaired-*t*-test with Bonferroni correction. ††$P < 0.01$ and †$P < 0.05$, SHR_{120} versus SHR_{160} by paired-*t*-test with Bonferroni correction. ‡‡$P < 0.01$, peripheral arc versus total baroreflex by paired-*t*-test in each group.

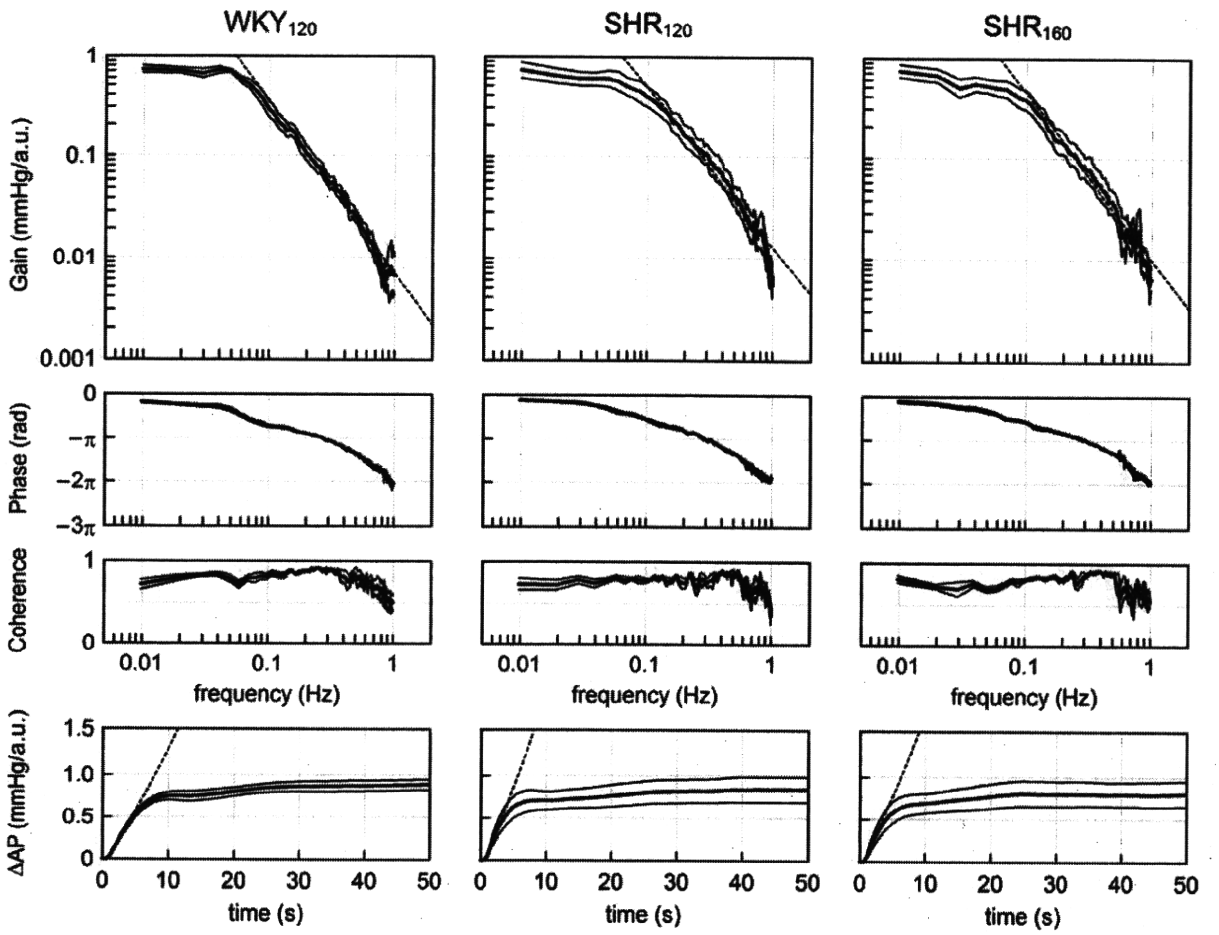

Fig. 3. Transfer functions of the baroreflex peripheral arc from SNA to AP averaged for WKY_{120}, SHR_{120} and SHR_{160} groups. Gain, phase, and coherence plots are shown. The dashed oblique line in the gain plot indicates G_{slope}. There is no significant difference in G_{slope} between WKY_{120} and SHR_{120} or between SHR_{120} and SHR_{160}. *Bottom*: step responses of AP calculated from the corresponding peripheral arc transfer functions. The dashed oblique line in the step response indicates the initial slope (S_{slope}) of the step response. There were no significant differences in S_{slope}. In all panels, the bold and thin lines indicate mean and mean ± SE values, respectively.

The total baroreflex transfer functions are depicted in Fig. 4. In the gain plots, the dynamic gain declined as the frequency increased above 0.05 Hz, indicating low-pass characteristics of the AP response to the CSP input. $G_{0.01}$, $G_{0.1}$, G_1, and G_{slope} did not differ significantly between WKY_{120} and SHR_{120} or between SHR_{120} and SHR_{160} (Table 2). The phase plots of three groups were also similar: the phase approached $-\pi$ radians at 0.01 Hz, reflecting the negative feedback operation attained by the total baroreflex. The phase was delayed as the frequency increased. For the step response, S_{50} and S_{slope} did not differ between WKY_{120} and SHR_{120} or between SHR_{120} and SHR_{160}. Within-group comparisons using paired *t*-test indicated that G_{slope} was significantly less negative in the total baroreflex than in the peripheral arc transfer function (Table 2).

The transfer functions from CSP to HR are shown in Fig. 5. In the gain plots, the dynamic gain decreased as the frequency increased. $G_{0.01}$ and $G_{0.1}$ were significantly smaller in SHR_{120} than in WKY_{120} (Table 2). Although $G_{0.01}$ did not differ between SHR_{120} and SHR_{160}, $G_{0.1}$ was significantly greater in SHR_{160} than in SHR_{120}. G_1 was not compared because coherence near zero and the phase with increased scatter suggested poor reliability of the estimated transfer functions above 0.8 Hz. In the phase plots, the phase approached $-\pi$ radians at 0.01 Hz, indicating that HR responded negatively to the CSP input. For the step responses, both S_{50} and S_{slope} were significantly less negative in SHR_{120} than in WKY_{120}, while S_{50} and S_{slope} did not differ significantly between SHR_{120} and SHR_{160}.

When the carotid sinus baroreflex was virtually closed by adjusting CSP to AP, mean AP (and thus mean CSP) in WKY was close to 120 mmHg and that in SHR was near 160 mmHg (Table 3). The mean HR and SNA in WKY under the baroreflex closed-loop conditions, however, seemed higher than those observed in WKY_{120}. Similarly, the mean HR and SNA in SHR seemed higher than those observed in SHR_{160}.

Data obtained from the supplemental protocol were summarized in Fig. 6 and Table 4. The gray lines indicate transfer functions derived from $WKY_{120\text{-}S}$, while the black lines indicate those derived from $WKY_{160\text{-}S}$. In the neural arc transfer function, dynamic gain values below 0.1 Hz tended to be lower in $WKY_{160\text{-}S}$ than in $WKY_{120\text{-}S}$. G_{slope} did not differ between $WKY_{120\text{-}S}$ and $WKY_{160\text{-}S}$. In the neural arc step response, S_{peak} did not differ significantly, and S_{10} was marginally attenuated in $WKY_{160\text{-}S}$ ($P = 0.06$). In the peripheral arc, parameters of the transfer function did not differ statistically between

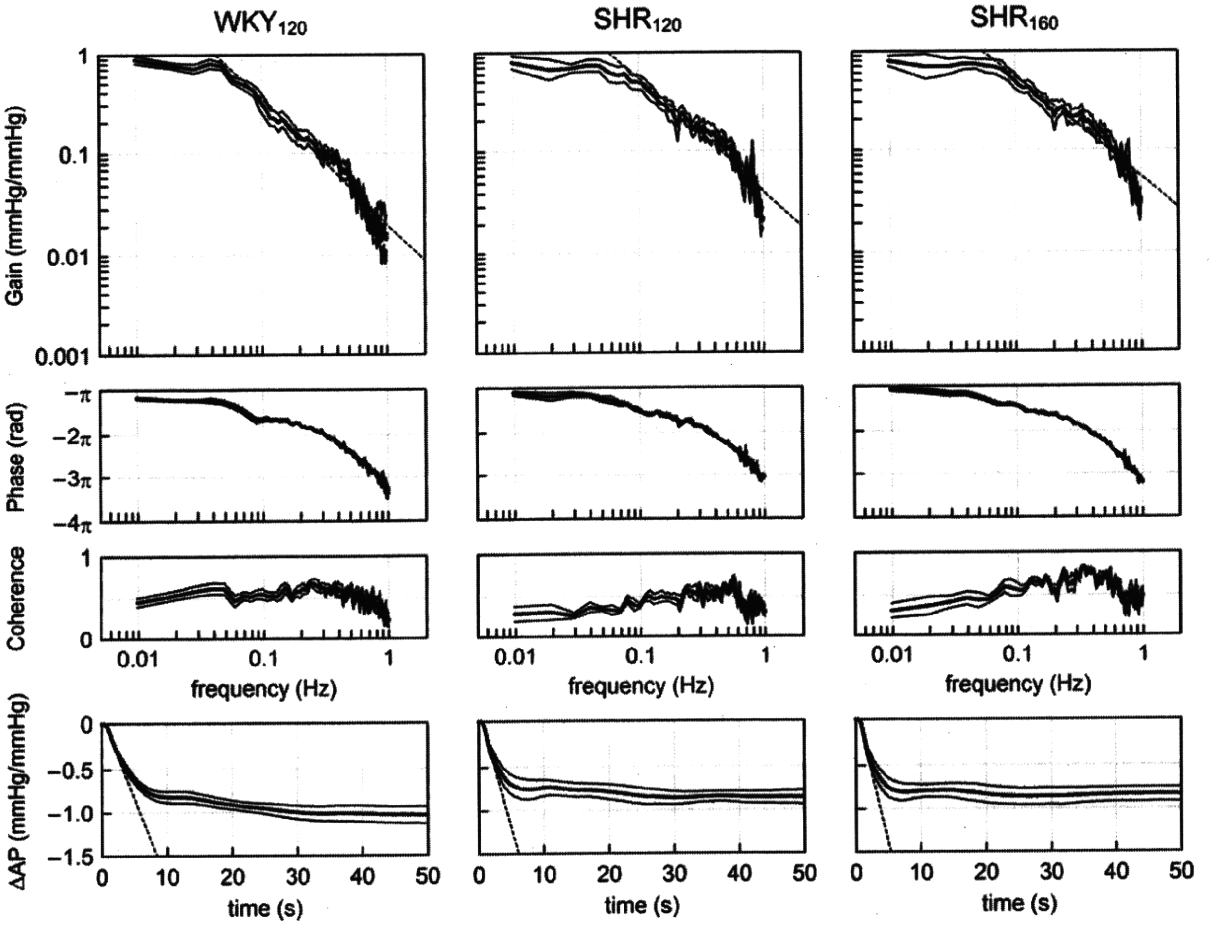

Fig. 4. Transfer functions of the total baroreflex from CSP to AP averaged for WKY_{120}, SHR_{120}, and SHR_{160} groups. Gain, phase, and coherence plots are shown. The dashed oblique line in the gain plot indicates G_{slope}. There is no significant difference in G_{slope} between WKY_{120} and SHR_{120} or between SHR_{120} and SHR_{160}. *Bottom*: step responses of AP calculated from the corresponding total baroreflex transfer functions. The dashed oblique line in the step response indicates the S_{slope}. There were no significant differences in S_{slope}. In all panels, the bold and thin lines indicate mean and mean ± SE values, respectively.

$WKY_{120\text{-}S}$ and $WKY_{160\text{-}S}$. In the peripheral arc step response, S_{slope} was significantly gentler in $WKY_{160\text{-}S}$. In the total baroreflex, although parameters of the transfer function did not differ statistically between $WKY_{120\text{-}S}$ and $WKY_{160\text{-}S}$, parameters of the step response, S_{50} and S_{slope}, were significantly attenuated in $WKY_{160\text{-}S}$.

DISCUSSION

In the present study, we comprehensively identified the open-loop transfer functions of the neural arc, peripheral arc, and total baroreflex in SHR using the normotensive WKY as a reference. Despite significant resetting of the baroreflex, the dynamic characteristics of AP regulation in SHR were comparable to those of WKY, except for a slight augmentation of the derivative characteristics of the neural arc at higher pressure input in SHR. On the other hand, the transfer function related to sympathetic HR control was significantly depressed in SHR compared with WKY.

Neural arc transfer function in SHR. The neural arc transfer function showed derivative characteristics in both WKY and SHR (Fig. 2), consistent with the findings of Harada et al. (7). The present results, however, differ slightly from the previous report in the following aspect. We demonstrated that G_1 and G_{slope} were significantly greater, and S_{peak} was significantly more negative in SHR_{160} than in SHR_{120}, indicating that higher pressure input enhanced the derivative characteristics in SHR. This was not simply an effect of the higher pressure input, because the higher pressure input did not increase G_1, G_{slope}, or S_{peak} in WKY (Fig. 6).

Both mechanosensory transduction at baroreceptors and central processing from baroreceptor afferent nerve activity to efferent SNA contribute to the generation of the derivative characteristics of the neural arc (16). According to a study by Brown et al. (1), the frequency response characteristics of aortic nerve discharge are similar between WKY and SHR in the frequency range of 0.1 to 20 Hz. Although direct comparison is difficult, the present results seem to be in line with their findings. Despite significant resetting in the static characteristics (24), dynamic characteristics of the carotid sinus baroreceptor transduction may not change appreciably in SHR.

Peripheral arc transfer function in SHR. There were no significant differences in the parameters of the peripheral arc transfer function between WKY and SHR (Fig. 3 and Table 2). A major neurotransmitter at the sympathetic nerve

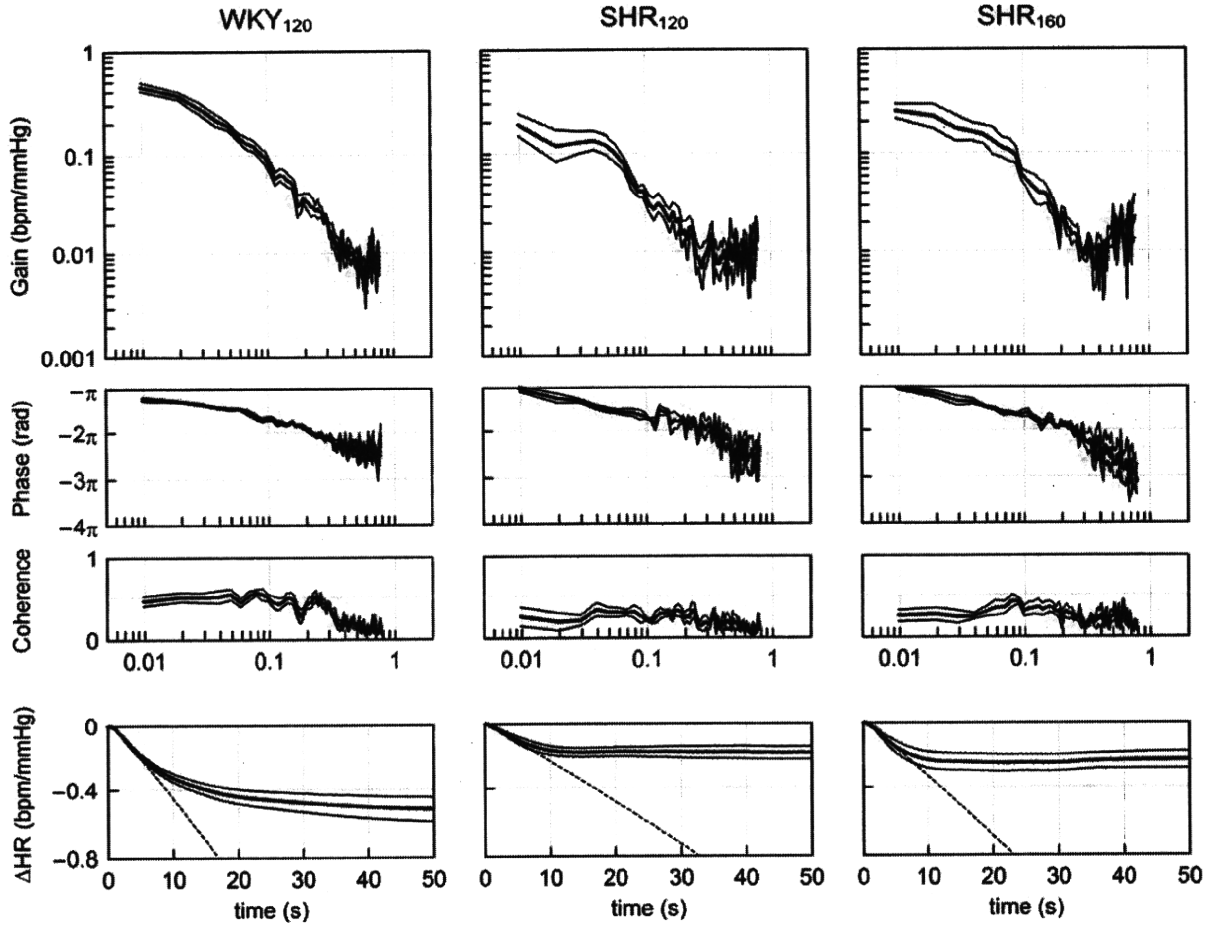

Fig. 5. Transfer functions from CSP to HR averaged for WKY_{120}, SHR_{120}, and SHR_{160} groups. Gain, phase, and coherence plots are shown. The dynamic gain values at 0.01 and 0.1 Hz are significantly smaller in SHR_{120} than in WKY_{120}. *Bottom*: step responses of HR calculated from the corresponding transfer functions. The dashed oblique line in the step response indicates S_{slope}. The steady-state step response and S_{slope} are significantly attenuated in SHR_{120} compared with WKY_{120}. In all panels, the bold and thin lines indicate mean and mean ± SE values, respectively.

endings is norepinephrine. The peripheral arc transfer function may thus reflect the combined dynamic properties of norepinephrine kinetics at the neuroeffector junction and the effector response to adrenergic stimulation (13). Neuronal uptake and α-adrenergic autoinhibition of norepinephrine operate to the same extent during electrical stimulation of the spinal cord in both SHR and WKY (36). Although norepinephrine uptake abnormalities have been reported in SHR (27, 28), the present results indicate that in this model, the influence of altered norepinephrine kinetics on the overall dynamic characteristics of the peripheral arc may be limited.

Table 3. *Mean AP, HR, and SNA under conditions of virtually closed baroreflex*

	WKY	SHR
Mean AP, mmHg	121 ± 3	156 ± 5**
Mean HR, bpm	414 ± 16	433 ± 13
Mean SNA, au	103 ± 14	130 ± 18

Data are presented in means ± SE (n = 7 for WKY and n = 6 for SHR). bpm, beats per minute; au, arbitrary unit. **$P < 0.01$ by unpaired-t-test.

In pithed rats, pressor response to electrical stimulation of the spinal cord is greater in SHR than in WKY (21, 36). Pressor response to norepinephrine or epinephrine is also enhanced in SHR (36). While the maximum pressor response to methoxamine is greater in SHR than in WKY, the pressor response to submaximal doses of methoxamine is attenuated in SHR (21). The present results suggest that the dynamic characteristics of the peripheral arc are not remarkably different between WKY and SHR despite possible differences in vascular sensitivity to adrenergic stimulation.

Total baroreflex transfer function in SHR. There were no significant differences in the parameters of the total baroreflex transfer function between WKY and SHR (Fig. 4, Table 2), even though AP was significantly higher in SHR than in WKY. In contrast, the step response of the total baroreflex was significantly attenuated in $WKY_{160\text{-}S}$ than in $WKY_{120\text{-}S}$ (Fig. 6, Table 4), indicating that the preservation of the total baroreflex function at the higher pressure input may be unique to SHR. In each of the WKY_{120}, SHR_{120}, and SHR_{160} groups, G_{slope} was significantly less negative in the total baroreflex than in the corresponding peripheral arc, suggesting an improvement of dynamic gain in the higher-frequency range of 0.1 to 1 Hz. The

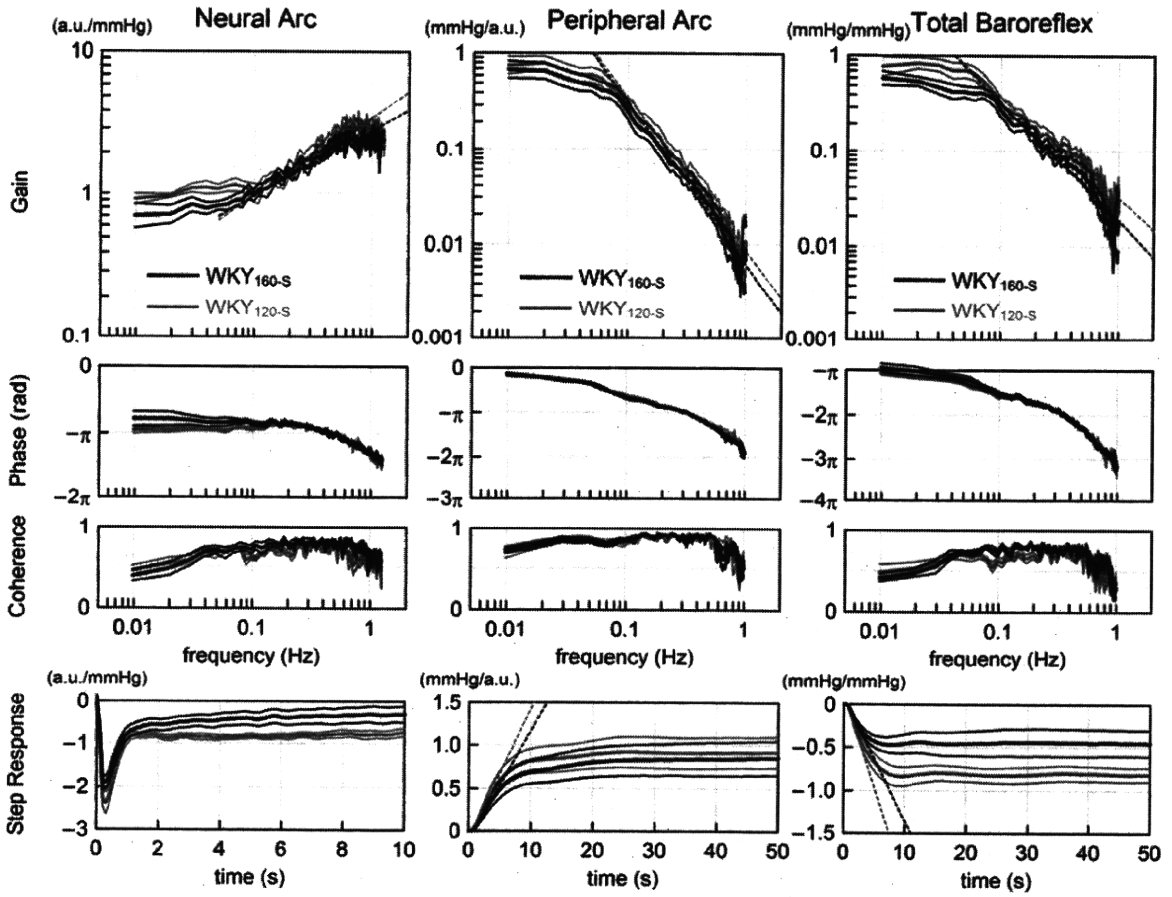

Fig. 6. Transfer functions of the neural arc, peripheral arc, and total baroreflex obtained from an additional protocol. In each panel, the gray lines indicate the transfer functions estimated from $WKY_{120\text{-}S}$. The black lines indicate the transfer functions estimated from $WKY_{160\text{-}S}$. No significant enhancement at the higher pressure input was observed in the derivative characteristics of the neural arc transfer function between 0.1 and 1 Hz. *Bottom*: step responses corresponding to the respective transfer functions. S_{slope} in the peripheral arc was significantly gentler in $WKY_{160\text{-}S}$ than in $WKY_{120\text{-}S}$. Both S_{50} and S_{slope} in the total baroreflex were significantly attenuated in $WKY_{160\text{-}S}$ than in $WKY_{120\text{-}S}$. In all panels, the bold and thin lines indicate mean and mean ± SE values, respectively.

neural arc may thus serve as an accelerating mechanism to improve the dynamic AP regulation in both WKY and SHR. Because G_{slope} in the neural arc was significantly greater in SHR_{160} than in SHR_{120} and G_{slope} in the peripheral arc did not differ between the two groups, G_{slope} in the total loop is expected to be less negative in SHR_{160}. This difference was not detected statistically, however, probably because an increase of G_{slope} by 2.4 dB/decade in the neural arc was partially offset by a decrease of G_{slope} by 1.4 dB/decade in the peripheral arc.

The well-preserved total baroreflex transfer function in SHR is in marked contrast to the significant depression of total baroreflex transfer function in chronic heart failure rats after myocardial infarction (12). Osborn (26) has demonstrated that sinoaortic denervation does not chronically increase mean AP in SHR, suggesting that the arterial baroreflex does not contribute much to the chronic regulation of mean AP in SHR. Nevertheless, the present results imply that the arterial baroreflex in SHR is still important for attenuating acute disturbances in AP.

Transfer function of HR control. In contrast to the total baroreflex transfer function, the transfer function of HR control showed significant depression in dynamic gain in SHR. Although the decreased baroreflex-mediated HR response is primarily attributed to a defect in parasympathetic control (29), the present results obtained in vagotomized rats indicate that the dynamic sympathetic control of HR may also be depressed in SHR. Despite the significant alteration in the sympathetic HR control, the total baroreflex transfer function did not differ between WKY and SHR, suggesting little contribution of HR to the determination of dynamic AP regulation. The lack of significant effect of HR on the dynamic AP regulation is consistent with the findings in rabbits (13, 25).

Baroreflex closed-loop conditions. In the present experimental settings, the baroreflex could be virtually closed by adjusting CSP to AP. The closed-loop operating AP (Table 3) provides a rationale for the selection of the mean input pressure of CSP. When CSP was perturbed around the operating-point pressure, however, mean SNA and AP usually decreased (10). The phenomenon may be related to the input pulsatility and the effect of input amplitude (3, 17, 35). Mean SNA and AP are expected to decrease as the input amplitude of CSP perturbation increases when the mean CSP is lower than the midpoint of the inverse sigmoidal curve characterizing the CSP-SNA relationship.